HYDROGELS AND AEROGELS BASED ON CHEMICALLY CROSS-LINKED CELLULOSE NANOCRYSTALS

By: Xuan Yang. B.Eng

McMaster University, yangx34@mcmaster.ca

A thesis Submitted to the School of Graduate Studies in Partial Fulfillment of the Requirements for the Degree Master of Applied Science

MASTER OF APPLIED SCIENCE (2014) McMaster University

(Chemical Engineering) Hamilton, Ontario

TITLE: Hydrogels and Aerogels Based on Chemically Cross-linked Cellulose Nanocrystals

AUTHOR: Xuan Yang, B.Eng (Zhejiang University, Hangzhou, China)

SUPERVISOR: Professor Emily D. Cranston

NUMBER OF PAGES: xiii, 100

Abstract

Cellulose nanocrystals (CNCs) make up a promising new class of renewable nanomaterials with unique properties including nano-dimensions, high strength, light weight, liquid crystalline behaviour, biodegradability and general biocompatibility. The objective of this work was to study the use of chemically cross-linkable cellulose nanocrystals in gels, specifically injectable hydrogels and aerogels.

First, aldehyde-functionalized CNCs (CHO–CNCs) were used to reinforce injectable hydrogels based on carboxymethyl cellulose and dextran. The mechanical properties, internal morphology, and swelling of injectable hydrogels with unmodified and modified CNCs at various loadings were examined. The maximum storage modulus was observed in hydrogels with 0.250 wt. % of unmodified CNCs and 0.375 wt. % of CHO–CNCs. CHO–CNCs acted as both a filler and a chemical cross-linker, making the CHO–CNC-reinforced hydrogels more elastic, more dimensionally stable, and capable of facilitating higher nanoparticle loadings, compared to hydrogels with unmodified CNCs. When immersed in purified water or 10 mM PBS buffer, all CNC-reinforced hydrogels maintained their original shape for more than 60 days. No significant cytotoxicity to NIH 3T3 fibroblast cells was observed for the hydrogels or their individual components. These properties make CNC-reinforced injectable hydrogels of potential interest for various biomedical applications such as drug delivery vehicles or tissue engineering matrices.

Next, chemically cross-linked "all-CNC" aerogels were prepared based on similar hydrazone cross-linking with hydrazide-functionalized CNCs ($NHNH_2$-CNCs) and CHO-CNCs. These ultra lightweight (5.6 mg/cm^3) and highly porous (99.6%) aerogels displayed bimodal pore distribution (mesopores <50 nm and macropores >1 μm). Chemically cross-linked CNC aerogels showed enhanced mechanical properties and shape recovery ability, particularly in water, compared to previous reports of physically cross-linked CNC aerogels. Specifically, the aerogel shape recovers at least 85% after 80% compressive strain, even after 20 compress and release cycles. These CNC aerogels can absorb significant amounts of both water (160 ± 10 g per g) and dodecane (72 ± 5 g per g) with cyclic absorption capacity. It is demonstrated that CNC aerogels may have application as superabsorbents and for oil/water separations.

Acknowledgements

Firstly, I would like to thank my supervisor, Dr. Cranston, for all her patient guidance, constant encouragement and helpful advice during my Master's study. She has given me enormous freedom to try different interesting projects so that I gained lots of useful research experience.

I would like to thank all the members of the Cranston Research Group for their help over these years. To Tiffany Abitbol, Kevin Kan, Heera Marway, Lexa Graham, Jonathan Monster, Joseph Pang, Anthony Palermo, Zhen Hu, Dan LeClair, Michael Reid, Stephanie Kedzior, without your useful discussions, suggestions and help, I would not have finished my Master's thesis successfully.

Special thanks to Dr. Hoare, Dr. Pelton, Dr. Zhu, Dr. Thompson, Dr. Stöver and Dr. Moran-Mirabal for the access to their instruments and expertise, and Ms. Emilia Bakaic, Ms. Elizabeth Takacs, Ms. Marcia Reid, Ms. Glynis de Silveira, Mr. Frank Gibbs, Mr. Steve Kornic and Mr. Emil Gustafsson for sample analysis or training.

Lastly, I would like to thank my friends and parents for the continuous support and encouragement. To my forever loved parents: thank you so much for supporting my studies abroad and exploring the "magic chemistry" area with me since my undergraduate studies.

Table of Contents

List of Figures

List of Tables

Nomenclature

AFM	Atomic Force Microscopy
ADH	Adipic Acid Dihydrazide
AGU	Anhydroglucose Unit
BC	Bacterial Cellulose
BET	Brunauer–Emmett–Teller
BJH	Barrett-Joyner-Halenda
CB[8]	Cucurbit[8]uril
CHO-CNCs	Aldehyde-modified CNCs
CMC	Sodium Carboxmethyl Cellulose
CMC-$NHNH_2$	Carboxymethyl Cellulose-hydrazide
CNCs	Cellulose Nanocrystals
CPD	Critical Point Drying
Dextran-CHO	Dextran-aldehyde
DLS	Dynamic Light Scattering
DMEM	Dulbecco's Modified Eagle Medium-high glucose
DMSO	Dimethyl Sulfoxide
EDC	N′-ethyl-N-(3-dimethylaminopropyl)-carbodiimide
EtOH	Ethanol or Ethyl alcohol
FBS	Fetal Bovine Serum
FTIR	Fourier Transform Infrared Spectroscopy
MTT	Thiazolyl Blue Tetrazolium Bromide
$NaIO_4$	Sodium Periodate
NFC	Nanofibrillated Cellulose
$NHNH_2$-CNCs	Hydrazide-modified CNCs
NHS	N-hydroxysuccinimide
PAA	Poly(acrylic acid)
PBS	Phosphate Buffered Saline
PDMAEMA	Poly(N,N-dimethylaminoethyl methacrylate)
PEG	Poly(ethylene glycol)
PEO	Poly(ethylene oxide)
PLA	Poly(lactic acid)
PNiPAAm	Poly(N-isopropylacrylamide)
PS	Polystyrene
PVA	Poly(vinyl alcohol)
SEM	Scanning Electron Microscopy
TEM	Transmission Electron Microscopy
TMOS	Tetramethoxysilane

Declaration of Achievement

I declare that the research contribution that follows represents original work, completed and written by myself, with editorial assistance from my supervisor, Dr. Cranston.

The MTT assays in Chapter 4 were done in collaboration with Ms. Emilia Bakaic and Dr. Todd Hoare.

Some parts of Chapter 2, 3 and 4 (related to injectable hydrogels) have previously been published, and are reproduced with permission from:

Yang, X., Bakaic, E., Hoare, T., Cranston, E. D. Injectable polysaccharide hydrogels reinforced with cellulose nanocrystals: morphology, rheology, degradation, and cytotoxicity. *Biomacromolecules* 14**,** 4447–55 (2013). Copyright © 2013 American Chemical Society.

CHAPTER 1: INTRODUCTION

1.1 Cellulose Nanocrystals in Gel Nanomaterials

Nanotechnology refers to the concepts and techniques used to make products with unique functionality based on their nano-scale properties. Nanomaterials have great potential for a vast range of applications including medicine, electronics, biomaterials and energy storage/production. A promising family of renewable nanomaterials is nanocellulose, in the form of nanofibrillated cellulose (NFC), cellulose nanocrystals (CNCs), and bacterial cellulose (BC) [1]–[3]. These polysaccharide nanoparticles can be obtained from cellulose - the most abundant renewable form of biomass in nature. With advantages over inorganic nanoparticles such as low cost, biocompatibility, biodegradability, good mechanical properties and chemically reactive surface functionality, nanocellulose has great potential for use in scaffolds, coatings, polymer composites, absorbents/adsorbents, and as rheological modifiers or emulsifiers, to name just a few.

A number of important programs aimed at the development and commercialization of nanocellulose products have recently begun worldwide including: the "Suomen Nanoselluloosakeskus Centre" or Finnish Centre for Nanocellulosic Technologies [4]; the "Nanocellulose, Rethink Paper" initiative driven by the US Department of Agriculture and the Technical Association of the Pulp and Paper Industry (TAPPI) [5]; and ArboraNano, a Canadian Business-led Networks of Centres of

Excellence program, joint with companies FPInnovations, CelluForce, Domtar and Alberta Innovates and strongly supported by the Canadian government [5]. Our Canadian program focuses on CNCs which are rigid rod-like nanoparticles with widths of a few nanometers and lengths ranging from hundreds of nanometers to microns. CNCs have recently become commercially available in Canada and the USA, as a result of various facilities which can now produce kg to tonne per day quantities with uniform properties and high purity.

The main objective for CNC research is to fully exploit the physical and chemical properties of CNCs in different applications. Due to CNCs' high specific strength and modulus, they have mainly been used as nano-fillers to reinforce different polymer matrices. Two challenges in developing new nanomaterials based on CNCs include (1) tuning the interactions between CNCs and polymer matrices and (2) achieving uniform distribution of CNCs. These are both significant because they will largely determine the mechanical performance of the final materials. Aside from mixing CNCs into polymer matrices, CNCs on their own can be assembled into films or gels in a controlled manner resulting in unique properties. The rod-like shape and nano-scale size of CNCs gives them the ability to behave like liquid crystals or entangled fibers, which can generate different nano-structures and lead to various final material properties and function.

A number of gel nanomaterials, such as hydrogels and aerogels, based on "bare" (unfunctionalized) CNCs have been studied [3], [6], [7]; however, only a few papers investigate the use of modified CNCs with the ability to form chemical cross-links. This

is the first work based on CNCs and hydrazone cross-linking, a rapid and initiator free cross-linking system. Studying the preparation, characterization and application of gels with chemically cross-linkable CNCs is meaningful: not only is it investigating new chemical modifications of CNCs on the nano-scale, but it leads to new properties and performance of materials on the bulk-scale. This fundamental research offers insight into the theory of gel reinforcement, which will hopefully guide the design of new materials to meet different application needs.

1.2 Research Objectives

The aim of this project is to study the use of chemically cross-linkable cellulose nanocrystals in gels, specifically injectable hydrogels and aerogels.

For injectable hydrogels:

This work seeks to investigate the use of cellulose nanocrystals as both nano-filler and cross-linker in an "all-polysaccharide" injectable hydrogel. We address (1) how the CNC concentration and cross-linking ability affects the mechanical properties, swelling and degradation behaviour of the hydrogels; and (2) the feasibility of using CNC-reinforced hydrogels in biomedical applications.

For aerogels:

The goal is to generate robust aerogels containing only cellulose nanocrystals. We present (1) the preparation of chemically cross-linked aerogels based on CNCs alone; (2) the characterization of CNC aerogels including density, specific surface area, pore

structure, mechanical properties and absorbance ability; and (3) potential applications of these unique aerogel nanomaterials such as superabsorbents and for oil/water separation.

1.3 Thesis Outline

The content of this thesis is divided into six chapters, including the Introduction. Chapter 2 of the thesis presents a literature review discussing the preparation, modification and unique properties of nanocellulose, specifically cellulose nanocrystals, as well as hydrogel and aerogels containing CNCs. Chapter 3 summarizes the materials and experimental procedures used in this research. Chapter 4 presents results and discussion of the injectable polysaccharide hydrogels reinforced with CNCs in which the morphology, rheology, degradation and cytotoxicity of the final hydrogels are studied. Chapter 5 presents results and discussion of chemically cross-linked "all-CNC" aerogels in which the morphology, mechanical properties and potential applications of the final aerogels are studied. Concluding remarks and suggestions for future work from each project are presented in Chapter 4 and Chapter 5, accordingly. Chapter 6 is a more general conclusion section for the entire thesis.

CHAPTER 2: LITERATURE REVIEW

2.1 Cellulose and Nanocellulose

Cellulose, a polysaccharide, is the most abundant renewable material on Earth. Approximately 5×10^{11} metric tonnes of cellulose are biosynthesized yearly, but only 2% is recovered and used industrially [8]. The cellulose polymer is composed of several hundred to over ten thousand β(1→4) D-glucose units (Figure 2.1), and each cellulose chain has a chemically reducing end (a hemiacetal unit) and a non-reducing end (with a pendant hydroxyl group) [3], [9]. Each anhydroglucose unit (AGU) consists of three hydroxyl groups, giving the cellulose molecule a high degree of functionality [10].

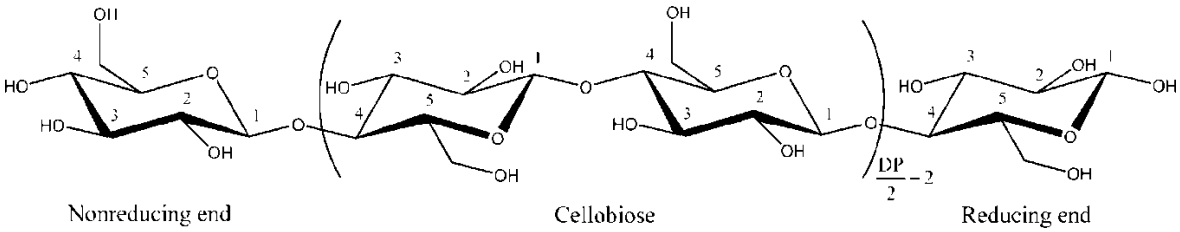

Figure 2.1. The chemical structure of cellulose. The repeat unit is called "cellobiose" which is composed of two β (1→4) linked D-glucose units. Figure reproduced from reference [3].

Generally, this fibrous, tough and water-insoluble biomacromolecule is an important component of the primary plant cell wall where it provides high tensile strength and flexibility. Figure 2.2 shows the wood hierarchical structure at different length scales: the whole tree (on the scale of meters), the cross-section (centimeters), growth rings (millimeters), cellular anatomy (tens of micrometers), layer structure within cell walls (micrometers), cellulose fibrils in a matrix mainly composed of hemicellulose and lignin

(tens of nanometers) and molecular structures of cellulose, hemicellulose, and lignin (nanometers) [11]. Cellulose is not only found in plants, but also in several marine animals (i.e., tunicates), and to a lesser degree in bacteria, algae, fungi, invertebrates and amoeba (protozoa) [3].

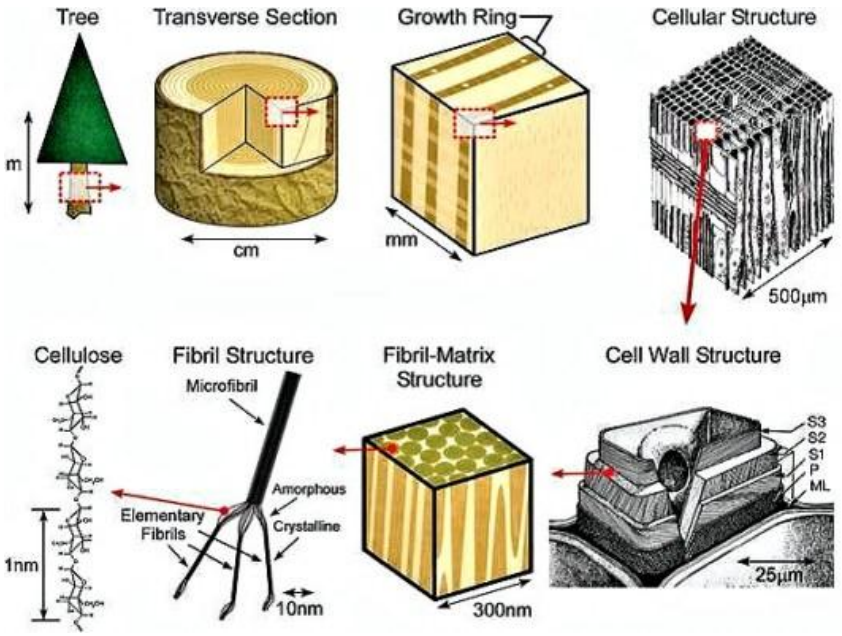

Figure 2.2. Cellulose structures in trees from logs to molecules. Figure reproduced from reference [11].

Due to cellulose's hydrophilicity, chirality, biodegradability and high functionality, both cellulose and cellulose derivatives have been widely studied and used for more than 150 years. Conventional applications of cellulose range from construction, food, paper, and biomaterials to pharmaceuticals [10]. Additionally, the increasing demand for products made from renewable, sustainable and non-petroleum based resources is also driving the development of new cellulose-based products.

2.1.1 Nanocellulose

Nanocellulose, in the form of nanofibrillated cellulose (NFC), cellulose nanocrystals (CNCs) and bacterial cellulose (BC), is a promising family of renewable nanomaterials with unique properties such as high strength, light weight, liquid crystalline behaviour, biodegradability and general biocompatibility [2], [3], [7], [12]. CNCs have also been referred to in the literature as cellulose nanowhiskers or nanocrystalline cellulose (NCC), and NFC is also sometimes called microfibrillated cellulose (MFC) or cellulose nanofibrils (CNF) [10], [12], [13]. Potential applications range from coatings, composites, absorbent products, rheological modifiers, emulsifiers, cosmetics to pharmaceuticals. The non-profit Canadian corporation FPInnovations estimates the nanocellulose market to be worth $250 million in North America by 2020 [5].

NFC, CNCs and BC are produced by different methods. To obtain NFC, mechanical treatments mainly consisting of high-pressure homogenization and/or grinding are used [1]. Acid hydrolysis is the most common method to obtain CNCs in which the acid preferentially degrades the amorphous regions and leaves the crystalline parts in-tact, isolating discrete CNC crystals [14]. Unlike NFC and CNCs which are both produced using a "top-down" approach from bulk cellulose, BC is produced using a "bottom-up" process whereby the bacterium *Gluconacetobacter xylinus* or the filamentous fungus *Trichoderma reesei* biosynthesize nanoscale ribbons which can be collected individually or as mats [15]–[17].

The preparation method, typical length, degree of crystallinity and unique properties of NFC, CNCs and BC are presented in Table 2.1, while typical transmission electron microscopy (TEM) images of these three are shown in Figure 2.3.

Table 2.1. Preparation method, length, degree of crystallinity and some unique properties of NFC, CNCs and BC.

	Nanofibrillated Cellulose (NFC)	**Cellulose Nanocrystals (CNCs)**	**Bacterial Cellulose (BC)**
Preparation Method	Mechanical treatment: high-pressure homogenization	Acid hydrolysis	Fermentation
Size-length (μm)	10-500	0.1-1	5-150
Crystallinity (%)	Similar to starting cellulose	80-90	70-90
Properties	Long length, Large aspect ratio	Short length, high crystallinity	Homogeneous, pure, free from lignin, pectin and hemicelluloses

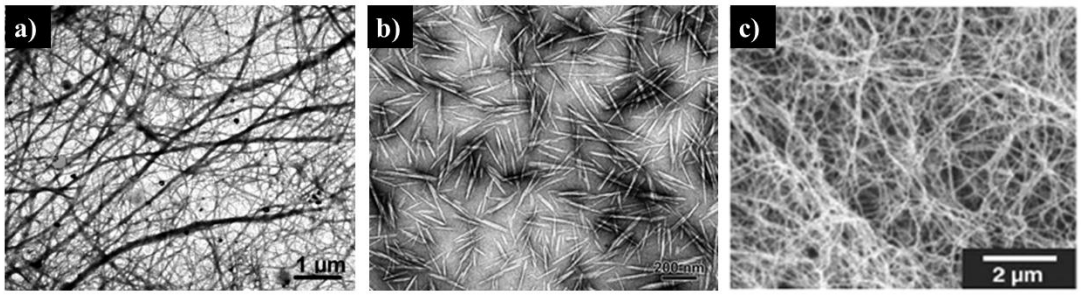

Figure 2.3. Transmission electron microscopy images of different nanocelluloses. (a) NFC made from Opuntia ficus-indicafibers [18], (b) CNCs from ramie fibers [19] and (c) BC from *Gluconacetobacter xylinus* [20].

In the nanocellulose family, cellulose nanocrystals and nanofibrillated cellulose are the most widely produced. There are several manufacturing facilities which have been, or are being built, that can produce up to tonnes per day of nanocellulose. Production has increased by 1000% in the past two years and will probably increase a further 500% by 2017 [5]. With more new manufacturing facilities and technologies, the cost will be controlled in an acceptable range (below $10/kg) in the future to further promote the use of nanocellulose in a variety of applications [21], [22]. This economic and environmentally friendly material is expected to render a significant contribution to technology in the 21st century [5].

2.2 Cellulose Nanocrystals

Cellulose nanocrystals are rigid rod-like particles with widths of a few nanometers and lengths ranging from hundreds of nanometers to microns, which have attracted significant attention in recent years. Compared with cellulose fibers, CNCs have advantages such as nanoscale lengths, high surface area, high specific strength and modulus. It should be mentioned that CNCs exhibit low cytotoxicity with a range of animal and human cell types [23]–[28] and are commercially available in Canada and the USA [5]. Additionally, CNCs have low ecotoxicological risk and their inhalation/oral toxicity and dermal irritation are minimal [23], [28]. As a result, CNCs have been approved as the first safe nanomaterial on Environment Canada's domestic substance list in 2013 [29], [30].

2.2.1 Preparation of Cellulose Nanocrystals

Cellulose nanocrystals are primarily produced by acid hydrolysis, which removes the amorphous regions and leaves the highly crystalline regions (Figure 2.4) [31], [32]. This procedure was first discovered in 1949 by Rånby in Sweden, and later developed in Canada [33]–[35]. Different hydrolysis and separation procedures have been established, which often depend on the starting cellulose source. Many reports describe CNCs from tunicate [31], [36], bacterial cellulose [37]–[39], ramie [19], [40], sisal [41], [42] pulp and cotton [43], [44]. The morphology of CNCs has most often been studied by atomic force microscopy (AFM), scanning electron microscopy (SEM), and TEM. Figure 2.5 shows the dimensions of CNCs from different cellulose sources.

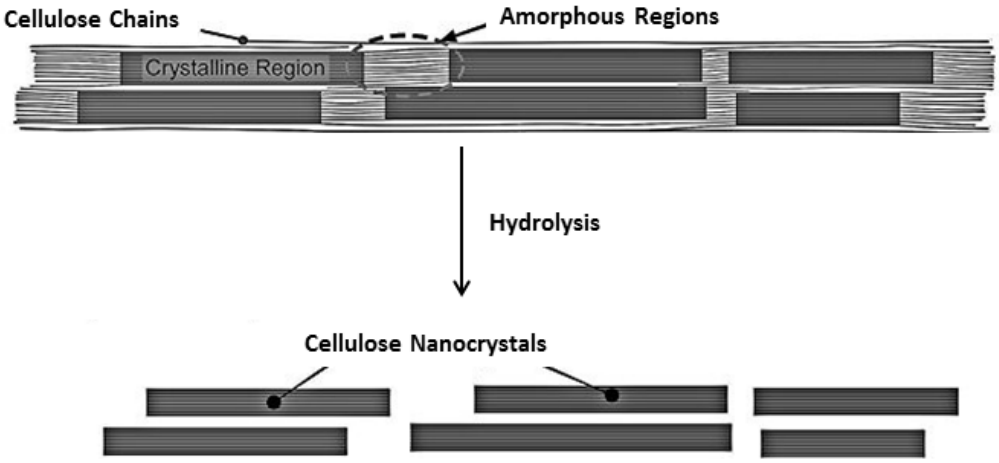

Figure 2.4. Schematic diagram illustrating the acid hydrolysis of cellulose. Figure reproduced from reference [45].

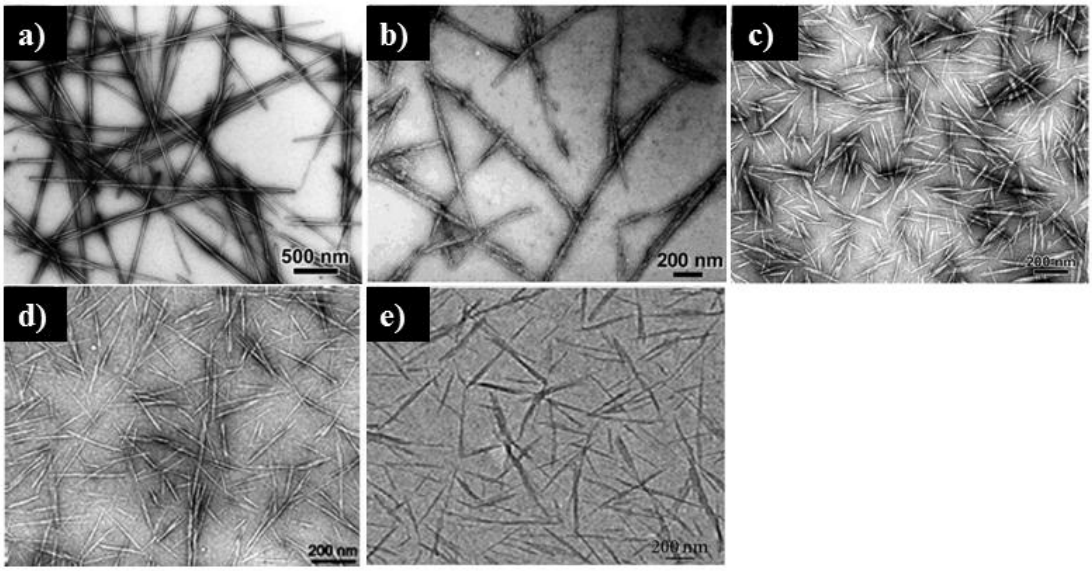

Figure 2.5. TEM images of dried dispersions of cellulose crystals from (a) tunicate [46], (b) bacterial cellulose [47], (c) ramie [19], (d) sisal [48] and (e) cotton [49]. Figure adapted from references [3] and [50].

Different acids can be used for CNC preparation such as sulfuric [14], hydrochloric [51], phosphoric [52], [53] and hydrobromic [54] acid. In our lab, we synthesize CNCs from cotton using the well-established sulfuric acid hydrolysis procedure [14]. Our CNCs are indistinguishable from those produced industrially from wood pulp and are highly crystalline with dimensions of 100-300 nm in length and 3-5 nm in diameter. In addition, the residual charged sulfate ester groups on the CNC surface, due to the H_2SO_4 hydrolysis process, promote the colloidal stability of CNCs in aqueous suspensions. CNCs can also be produced by ammonium persulfate oxidation, resulting in CNCs with similar dimensions and crystallinity, but with carboxylic acid groups on the surface instead of sulfate ester groups [55].

2.2.2 Chemical Modification of Cellulose Nanocrystals

Due to the abundant surface hydroxyl groups on CNCs, a numbers of chemical modifications have been studied such as TEMPO-mediated oxidation [25], [56], [57], esterification [58]–[60], silylation [61] and polymer grafting [43], [62]–[64]. Figure 2.6 summarizes some of the most common surface functionalizations reported. Most chemistries focus on (1) introducing stable negative or positive charges on the CNCs' surface to obtain better dispersion and (2) changing the surface functional groups to improve compatibility in nonpolar or hydrophobic solvents and matrices for nanocomposite development [3]. The challenge during these modifications is to change the surface chemistry of CNCs without damaging the original morphology. Additionally, "greener" procedures using less toxic chemicals and solvents are preferred.

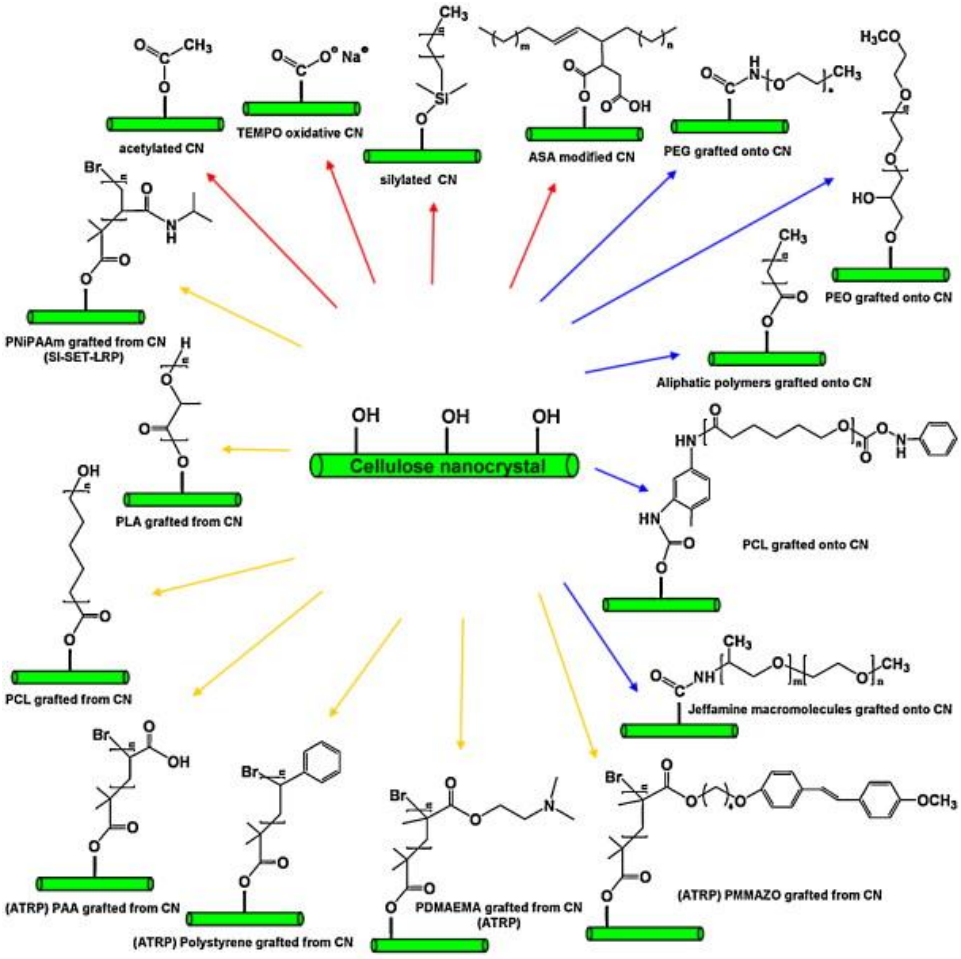

Figure 2.6. Common surface covalent chemical modifications of cellulose nanocrystals. PEG: poly(ethylene glycol); PEO: poly(ethylene oxide); PLA: poly(lactic acid); PAA: poly(acrylic acid); PNiPAAm: poly(N-isopropylacrylamide); PDMAEMA: poly(N,N-dimethylaminoethyl methacrylate). Figure reproduced from reference [65].

2.3 Cellulose Nanocrystal Gels

Gels are defined as substantially dilute cross-linked systems, which exhibit no flow in the steady-state [66]. In the past decades, many researchers have reported different gel nanomaterials with mechanical properties ranging from soft and weak, to hard and tough, making gels suitable for applications such as organic ceramics, catalyst substrates, coatings and composites [67]. Instead of using traditional synthetic polymers,

some researchers are focusing on using bio-sourced polysaccharides to form gels which have potential applications in biomaterials, food products and water purification.[68].

As a crystalline form of polysaccharide, cellulose nanocrystals have gained attention in gels due to their nano-scale dimensions and favourable mechanical properties. Generally, researchers use CNCs in gels for one of their three possible roles: (1) as nano-fibers which can entangle with each other to form a networked structure, (2) as liquid crystals which organize into a chiral nematic liquid crystalline phase and act as a substrate or template, or (3) as a nano-filler which can percolate through a polymer matrix to reinforce the gel system. Since the use of CNCs in gel nanomaterials is still in its early stages, there are many areas to explore from fundamental science to applied engineering.

2.3.1 CNCs Alone as Nano-Fibers

Cellulose nanocrystals themselves will entangle and form physical cross-links with each other to form a gel network under certain conditions. Figure 2.7 shows that a suspension of CNCs with either carboxylic acid or amine moieties will gel when the pH is changed, since the attractive forces based on hydrogen bonding will dominate the interactions between the deprotonated CNCs [69]. With proper drying methods, these hydrogels will turn into aerogels. However, in order to get a good networked structure, relatively high concentrations of CNCs (above 4 wt. %) are needed to supply efficient percolation abilities or cross-links.

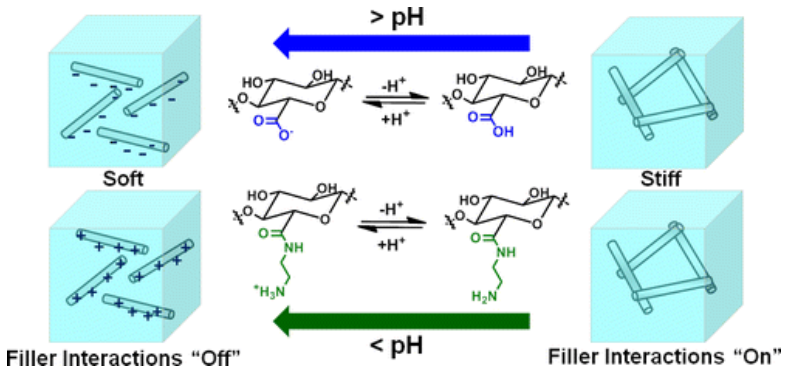

Figure 2.7. Schematic diagram illustrating the pH-responsive transition of gelation of cellulose nanocrystals with either carboxylic acid or amine moieties. Figure reproduced from reference [69].

2.3.2 CNCs in Other Matrices as Liquid Crystals

Cellulose nanocrystals can be used as templates to obtain nanomaterials with chiral nematic structure, since CNCs will organize into a chiral nematic liquid crystalline phase where the rod-shaped nanocrystals adopt a left-handed helical structure in a good solvent such as water. Figure 2.8 shows one example: the preparation of CNC/silica composite films through self-assembly of CNCs with tetramethoxysilane (TMOS) [70]. Besides this work, Dr. MacLachlan's group at UBC has also demonstrated that CNCs can be used to template a variety of different mesoporous materials with chiral nematic structures such as silica [70]–[72], photonic resins [73], photonic hydrogels [74] and carbon [75]. In the final step, CNCs are removed giving unique optical properties and a porous structure which has been proposed for optical filters, chemical sensors, and mesoporous membranes for molecule separations. However, in order to obtain chiral nematic phases, a high concentration of CNC suspensions (above 6 wt. %) is needed which is expensive when compared to composites which tend to incorporate less than 5 wt. % CNCs. Furthermore, the chiral-templated materials suffer from poor mechanical

properties making it difficult to obtain large pieces which are needed for commercial applications.

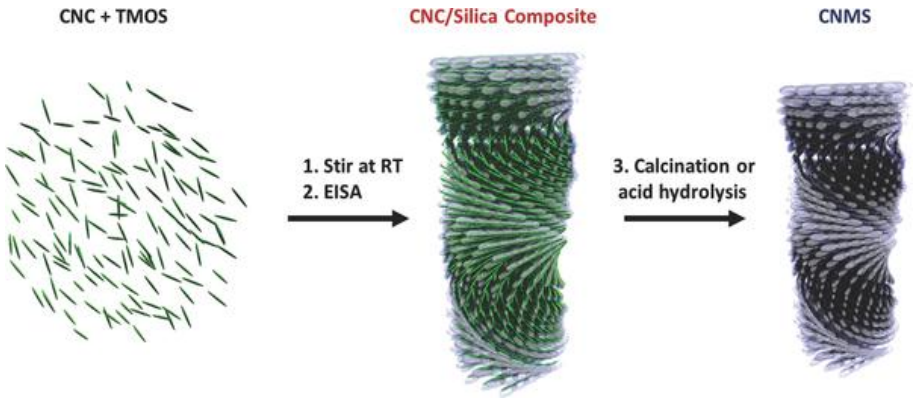

Figure 2.8. Preparation of chiral nematic structured CNC/silica Composites. Figure reproduced from reference [70].

2.3.3 CNCs in Other Matrices as Nano-Fillers

Aside from taking advantage of the liquid crystalline properties of CNCs, the introduction of CNCs as a nano-filler in a gel network can also modify gel performance. As shown in Figure 2.9, cellulose nanocrystals can be mixed into other polymer matrices forming gel networks. The choices of different CNCs (different aspect ratio or surface modifications), different polymer matrices and different preparation methods are the main factors that affect the properties of the final CNC gel.

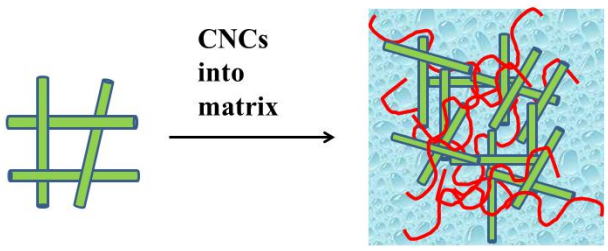

Figure 2.9. Schematic illustration of using cellulose nanocrystal as a nano-filler to reinforce a polymer matrix.

2.4 Hydrogels and Injectable Hydrogels

Hydrogels are a form of solid, yet jelly-like, networked polymeric materials. They are a subclass of gels with solvent distributed throughout the whole system. According to the type of cross-links, hydrogels are commonly classified as either physical or chemical hydrogels. Hydrogels are used widely in drug delivery and tissue engineering because of their highly hydrated three-dimensional porous structure which mimics biological tissue.

Injectable hydrogels are a subclass of hydrogels which can be prepared *in situ* by extruding hydrogel components from a syringe directly to the desired location, i.e., a mold, a cavity or even *in vivo*. Injectable hydrogel solution components instantly form physical or chemical cross-links upon contact, forming a gel. Furthermore, drugs, proteins, cells and nanoparticles can be mixed into the component solutions before injection; provided the gelation chemistry used is largely orthogonal with functionalities on the drug, protein, or cell, these components can be easily encapsulated within the hydrogel matrix as it forms. As such, for medical applications, no invasive surgical procedures are needed to insert gels with improved functionality into the body [76]–[78]. Injectability of hydrogels *in vivo*, has been successfully reported by various researchers [79]–[81] and injectable hydrogels with controllable degradability are promising for clinical use because degraded polymers are easily excreted by the human body [81], [82]. However, most injectable hydrogels reported in the literature have relatively low elastic moduli [83]–[85],

a potential limitation in some long-term biomedical applications (particularly in tissue engineering).

2.4.1 Hydrogels Reinforced by Nanoparticles

Previous studies have investigated hydrogels reinforced with nanoparticles such as laponite [86], silica [87]–[89], hydroxyapatite [90] and superparamagnetic iron oxide [80], which generally result in composite hydrogels with improved mechanical properties. The main challenge associated with the use of these inorganic nanoparticles *in vivo* is their potential toxicity and uncertain (or non-existent) mechanism of ultimate clearance from the body. Organic-based fillers may mitigate these disadvantages. More specifically, organic cellulose nanocrystals are promising organic fillers since they have been approved to be highly biocompatible materials as mentioned in Section 2.2.

2.4.2 Hydrogels Reinforced by Cellulose Nanocrystals

CNCs have favourable mechanical properties that make them ideal for applications where they are the load-bearing component in nanocomposites [91]. These include a Young's modulus of over 100 GPa, a large aspect-ratio, and a surface area of several hundred square meters per gram [2], [12], [92]. Previously, CNCs have been incorporated as fillers to reinforce polymer hydrogels (i.e., with no covalent attachment to the hydrogel) based on poly(acrylic acid) [93], poly(vinyl alcohol) (PVA) [94], α-cyclodextrin [95], poly(ethylene glycol) [96], PNiPAAm [97] and carboxymethyl cellulose/hydroxyethyl cellulose [98]. In all of these systems, improved mechanical properties were observed even at low CNC loadings (generally under 3 wt. %). However,

none of these hydrogels were injectable/*in situ* gellable and relatively few investigations into the internal structure and distribution of CNCs within the composites have been undertaken.

In most demonstrations of CNC-reinforced hydrogels, "bare" CNCs are physically entrapped within the gel matrix to yield the mechanical strength enhancement. A few papers have instead shown that CNCs with particular surface modifications can act as both filler and cross-linker to reinforce hydrogel systems. Recently, Dash *et al*. [99] obtained gelatin-based hydrogels cross-linked by CNCs oxidized to impart aldehyde-functionality; the amine groups on gelatin could then react with the aldehyde groups on the CNCs. However, these hydrogels needed to be dried for 24 h and stored at 4 ^{o}C for 10 days before usage, making them impractical as injectable therapeutics. Zhou *et al*. [100] found that CNCs could act as multifunctional cross-linkers to reinforce polyacrylamide hydrogels during *in situ* free-radical polymerization, using potassium persulfate (KPS) to initiate radicals on the surface of the CNCs which then participated in the polyacrylamide polymerization. Similarly, Hebeish *et al*. [101] developed PNIPAm hydrogels with CNCs chemically embedded in the matrix in the presence of cross-linker (methylene bis acrylamide). Yang *et al*. [102] covalently bound alkene-modified CNCs into poly(acrylic acid) hydrogels via copolymerization to achieve reinforcement. However, in the latter three examples, the small molecule free radical initiator KPS was used and a heating step was required to produce the gel, making these approaches unsuitable for most biomedical applications. Instead, McKee *et al*. [103] reported a PVA hydrogel using modified CNCs as cross-linkers based on supramolecular cucurbit[8]uril (CB[8]) cross-link chemistry

(Figure 2.10). However, the modification of CNCs by this route is complicated which may limit its practical application.

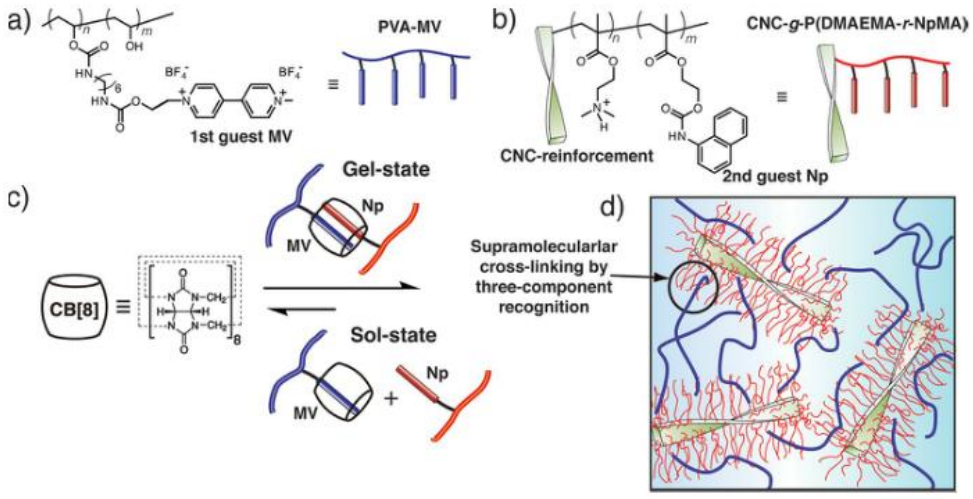

Figure 2.10. Schematics and architecture for highly specific, dynamic and stiff, three-component recognition-driven supramolecular hydrogels based on cellulose nanocrystals and CB[8] host-guest chemistry. Figure reproduced from reference [103].

2.5 Aerogels

Aerogels are highly porous materials derived from gels, in which the liquid component of the gel has been replaced by gas. In 1931, S. Kistler synthesized the first aerogel from various materials including alumina, rubber, silica and cellulose derivatives [104]. The method he used was called critical point drying (CPD), and is still actively used today. In the CPD method, a hydrogel is formed initially, which is then solvent exchanged with ethanol (or another water-soluble alcohol). Then the alcogel is dried under supercritical conditions to form the aerogel. In addition to the CPD method, lyophilization (freeze-dying) is also widely used to obtain aerogels where the hydrogel is

frozen and dried under high vacuum. Both CPD and lyophilization are generally able to remove the liquid from a gel without entirely collapsing the network structure.

Currently, aerogels based on silica have been the most widely studied due to their high porosities (up to 99%), low density (0.004 to 0.500 g/cm^3) and large surface areas (100 to 1000 m^2/g) [105]. Applications vary from catalysts [106], [107], super-thermal insulation [108], sound insulators [109] to electronics [110]. However, aerogels based on silica suffer from fragility which limits their use in application where robustness is needed. Aerogels based on synthetic polymers or native cellulose have been proposed as one solution to overcome this problem since they are generally less brittle, more flexible and easy to process/handle [111]. Compared with synthetic polymers derived from the oil industry and declining petrochemical sources, renewable biopolymers like cellulose, are an economic and environmentally-friendly choice.

2.5.1 Aerogels Based on Nanocellulose

A number of aerogels based on nanocellulose have been described in the literature and have the advantage of significantly higher surface area and controllable pore structure, when compared to aerogels based on bulk cellulose or pulp fibers. Among them, aerogels based on nanofibrillated cellulose are the most common [112]–[122]. Not only do they have unique fibrillar morphology from the long nanofibers, but they have good mechanical properties which result naturally from a combination of fibril entanglement and strong van der Waals interactions and hydrogen bonding. NFC aerogels usually display ultralow densities, high surface areas, and reasonable mechanical properties [115],

[121]. They can be used for different applications such as oil absorbents [113], [114], [116], [118]–[120], filters [111] and antibacterial agent substrates [122].

Other than aerogels based on NFC, aerogels made by bacterial cellulose have also been reported. For example, Haimer *et al*. [123] prepared bacterial cellulose aerogels which can be used as a bioactive compound release systems; Wu *et al*. [124] reported an ultralight and flexible bacterial cellulose aerogel which has potential as a supercapacitor, catalyst support and advanced sensor.

Compared with NFC and BC, CNCs have enhanced mechanical properties due to their high crystallinity and are the only member of the nanocellulose family approved as safe by various standards [29], [30]. Thus aerogels based on CNC are promising to be used when strength/stiffness is required and as biomaterials.

2.5.2 Aerogels Based on Cellulose Nanocrystals

Unlike NFC or BC, which have lengths up to several microns, it is difficult to build up aerogels containing only cellulose nanocrystals due to inefficient entanglement between CNC particles. To the best of our knowledge, only a few studies have been done on "all-CNC" aerogels: Fumagalli *et al*. [125] reported a CNC aerogel prepared by freeze-drying a CNC suspension in a water and *tert*-butanol (t-BuOH) mixture; Heath *et al*. [126] reported a CNC aerogel prepared from a CNC hydrogel by the CPD method; Dash *et al*. [127] reported a CNC aerogel by freeze casting CNC suspensions. Table 2.2 shows the basic information about these three works, thus summarizing the current CNC aerogel literature.

Table 2.2. Preparation method, CNC starting concentration, density and pore size (or inter-lamellar space) of "all-CNC" aerogels reported in the literature.

	Fumagalli *et al*. [125]	**Heath *et al*.** [126]	**Dash *et al*.** [127]
Preparation Method	Lyophilization	CPD	Freeze casting
CNC starting concentration (wt. %)	2	8 - 16	2
Density (mg/cm^3)	Not reported	78 - 155	22-31
Pore size or Inter-lamellar space (μm)	Not reported	> 5*	10 – 100
Specific surface area (m^2/g)	Up to160	Not reported	78 - 605

* Pore size was measured based on SEM images from reference [126].

In the work by Fumagalli *et al*. [125], CNC suspensions in mixtures of water and t-BuOH were freeze-dried into aerogels with high specific areas (up to 160 m^2/g) and a widely open texture. After gas-phase palmitoylation, the final CNC aerogels can be readily dispersible into hydrophobic non-polar liquids to yield non-flocculating suspension, which was a new way to achieve surface hydrophobization of CNCs. However, no detailed measurement of aerogel density or pore structure was undertaken.

In the work by Heath *et al*. [126], CNC suspensions (with concentrations above 8 wt. %) were sonicated under high frequency power until gelation occurred. Then, the CNC hydrogel was solvent exchanged with ethanol and dried by CPD. The final aerogel displayed impressive properties like density as low as 78 mg/cm^3 and specific surface area up to 605 m^2/g. However, this method required a high starting concentration of CNCs and high power sonication. Additionally, the ultrasound gelation kinetics and

process are not entirely clear and the authors propose that further investigations are needed.

In the work by Dash *et al*. [127], a freeze casting method was used (Figure 2.11a). A CNC suspension was placed into an insulating container with liquid nitrogen at the bottom, then the CNC network was formed around the growth of ice crystals. Interestingly, the aerogel showed a lamellar channel structure in the vertical direction. This arose because the ice crystals grow in the same direction as the temperature gradient and CNCs are excluded from, and then trapped between, the ice crystals; the lamellar channels can be preserved after removing the ice crystal templates through freeze drying (Figure 2.11b).

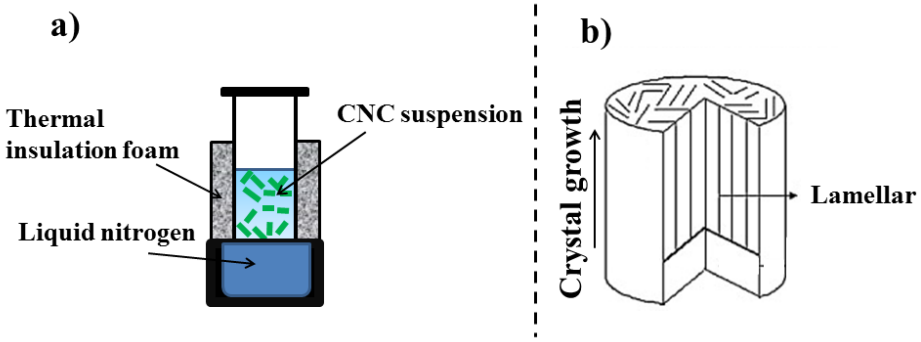

Figure 2.11. Schematic diagram of (a) freeze casing method to prepare CNC aerogels and (b) the growth pattern of ice crystals. Figure adapted from reference [127].

Figure 2.12 shows SEM images of the CNC aerogels which have a pore size above 5 µm. Although the aerogels from Heath *et al*. show much smaller pores under 200 nm (Figure 2.12b), the pores structure is not uniform. In fact, rather than obtaining entanglements or networks based on individual CNCs, these aerogels were based on sheets of CNCs which assemble into a network structure with pore size dependent on the

size of ice crystal templates during the freezing procedure. As a consequence, CNC aerogels presented to date have only macropores (pore diameter > 1 μm) which implies that some of the advantages of using nano-sized CNCs as a starting material is lost.

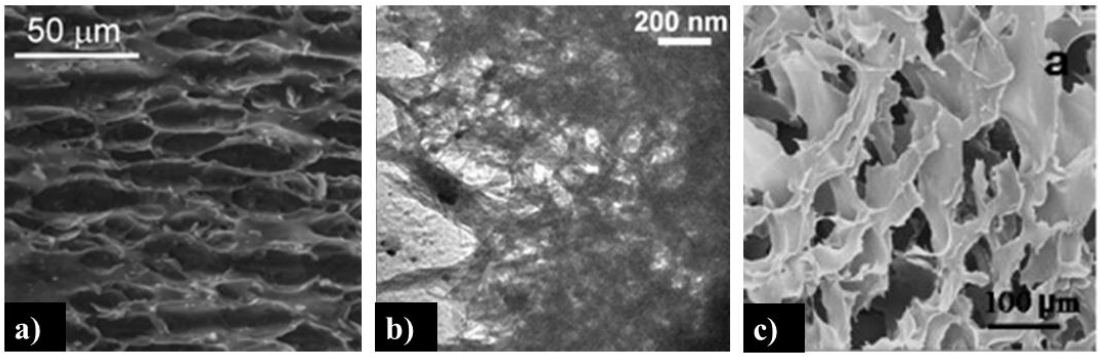

Figure 2.12. SEM images of CNC aerogels by different researchers: (a), (b)Heath *et al*. [126] and (c) Dash *et al*. [127].

In these CNC aerogel reports, a discussion of the mechanical properties and the ability to use these aerogels in water environments is often omitted [126], [127]. There is reasonable concern that "all-CNC" aerogels with only hydrogen bonding physical cross-links may suffer from poor mechanical performance and may collapse or re-disperse in water.

To the best of our knowledge, no chemically cross-linked CNC aerogels have been studied which we anticipate may have better mechanical properties due to covalent bonds which are stronger than physical cross-links, van der Waals and hydrogen bonds. Also, the chemically cross-linked networks may generate smaller pores and impart unique properties such as better absorption capacity.

2.6 Hydrazone Bonds as Chemical Cross-Links

As mentioned before, gel networks can be formed by either physical or chemical cross-linking. Compared with physically cross-linked gels, chemically cross-linked gels with higher mechanical strength and more controllable degradation and clearance are more suitable for long-term biomedical applications.

Different chemistries have been created to obtain chemically cross-linked gels which can be used as biomaterials, in which gelation would happen under normal conditions without toxic initiators. Patenaude *et al*. reported a disulfide bond chemistry which can generate hydrogel networks [128]. Li *et al*. reported a 1-4 addition chemistry between a nucleophile (i.e., thiol group) and a carbonyl compound (i.e., ketone or aldehyde) which can also have stable gelation [129]. However, gelation rates for both cases are generally considered too slow when quick-gelling properties are needed. Ossipov *et al*. created a oxime bond chemistry between a hydroxylamine group and an aldehyde group, however it required an acid catalyst to get a fast cross-linking rate which limit its application to acidic environments [130].

Hydrazone cross-linking chemistry between a hydrazide (or hydrazine) and a carbonyl group (i.e., ketone or aldehyde) stands out since it has a fast gelation time (within seconds) and when used in hydrogels leads to materials with good mechanical property and low toxicity [79], [81], [131]. Figure 2.13 shows the formation of a hydrazone cross-linked hydrogel network from aldehyde and hydrazide functionalized precursors [131]. To the best of our knowledge, hydrazone chemistry has not been used

for CNC gels which are normally based on physical interactions. The introduction of this unique chemistry into CNC gel systems (both injectable hydrogels and aerogels) will bring new properties to the final gel materials such as the possibility to have injectability, *in situ* gelling, enhanced mechanical properties and low toxicity.

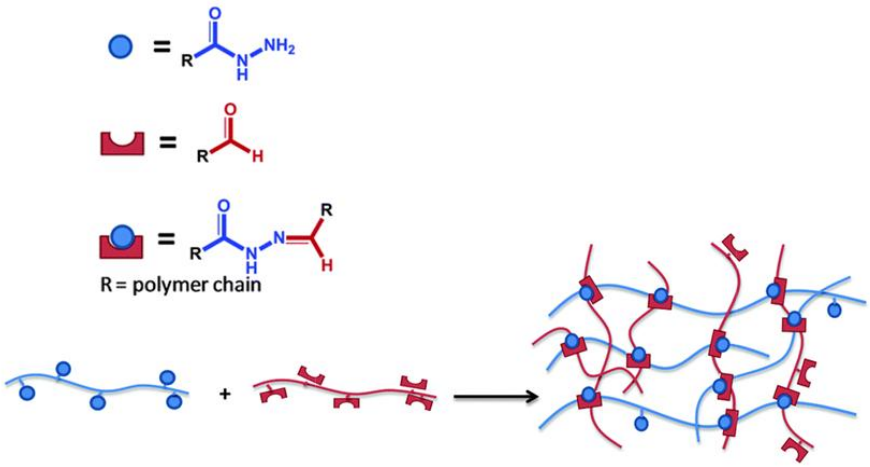

Figure 2.13. Hydrogel formation from hydrazone cross-links. Figure reproduced from reference [131].

CHAPTER 3: EXPERIMENTAL PROCEDURES

3.1 Materials

Whatman cotton ashless filter aid was purchased from GE Healthcare Canada, and sulfuric acid (95 ~ 98%) was purchased from VWR Canada. Sodium carboxmethyl cellulose (CMC) (M_w ~250 000, DS = 0.9), dextran from *Leuconstoc spp.* (M_r = 500 000), adipic acid dihydrazide (ADH, 98%), N-hydroxysuccinimide (NHS, 97%), N′-ethyl-N-(3-dimethylaminopropyl)-carbodiimide (EDC, commercial grade), ethylene glycol (99.8%), silver(I) oxide (≥99.99% trace metals basis), sodium chloride (≥99.5%), sodium periodate ($NaIO_4$, >99.8%) nile blue dye (≥75%) and dodecane (≥99%) were all purchased from Sigma Aldrich (Oakville, ON, Canada). Anhydrous ethyl alcohol (EtOH) was purchased from Commercial Alcohols Inc. Sodium hydroxide was purchased from EMD Millipore Germany, and hydrogen chloride was purchased from LabChem Inc.

Cellulose nanocrystals with surface carboxyl groups (COOH-CNCs) were prepared by oxidation of cotton with ammonium persulfate and were supplied by BioVision, Inc (New Minas, NS, Canada) [55]**.** All water used was purified Type I water with a resistivity of 18.2 MΩ cm (Barnstead NANOpure DIamond system, Thermo Scientific, Asheville, NC). Dimethyl sulfoxide (DMSO, reagent grade) was purchased from Caledon Laboratory Chemicals (Georgetown, ON, Canada). NIH 3T3 *Mus musculus* mouse fibroblast cells were obtained from ATCC: Cederlane Laboratories (Burlington, ON, Canada). Cell proliferation media, recovery media, and trypsin-EDTA were obtained from Invitrogen (Burlington, ON, Canada). Media contents included Dulbecco's Modified Eagle Medium-

high glucose (DMEM), fetal bovine serum (FBS), horse serum (HS), and penicillin streptomycin (PS). Thiazolyl blue tetrazolium bromide (MTT) was purchased from Sigma Aldrich (Oakville, ON, Canada).

3.2 Preparation of Carboxymethyl Cellulose-Hydrazide and Dextran-Aldehyde

Carboxymethyl Cellulose-Hydrazide Synthesis (CMC-$NHNH_2$). 1.0 g of CMC and 3 g of ADH were dissolved sequentially in a 500 mL flask with 200 mL of purified water. 0.07 g of NHS was suspended in 4 mL of a 1:1 DMSO:H_2O solution. 0.3 g of EDC was dissolved in 1 mL of a 1:1 DMSO:H_2O solution. NHS solutions and EDC solutions were added dropwise to the flask sequentially. The pH of the CMC-$NHNH_2$ solution was then adjusted to pH 6.8 using NaOH and HCl solutions until the pH of the solution no longer rapidly changed. The solution was dialyzed (dialysis membrane molecular weight cut-off 12-14,000 Da, VWR Canada) for a minimum of six water changes, over which the water volume was approximately 100 times the volume of the dialysate. Finally, CMC-$NHNH_2$ was lyophilized.

Dextran-Aldehyde Synthesis (Dextran-CHO). 1.5 g of dextran was dissolved in 150 mL of purified water in a 500 mL flask. 0.8 g of $NaIO_4$ was dissolved in 10 mL of purified water and added dropwise to the dextran solution. The mixture was allowed to stir for 2 h at room temperature before 0.4 mL of ethylene glycol was added. The solution was allowed to stir for an additional hour to consume excess oxidizing agent. The solution was dialyzed (dialysis membrane molecular weight cut-off 12-14,000 Da) for a

minimum of six water changes, over which the water volume was approximately 100 times the volume of the dialysate. Finally, dextran-CHO was lyophilized.

3.3 Preparation of Modified Cellulose Nanocrystals

3.3.1 Preparation of Cellulose Nanocrystals

CNCs were obtained from the acid hydrolysis of cotton ashless filter aid using 64 wt. % sulfuric acid at 45 °C for 45 min, as described previously [14]. The CNC precipitate was then rinsed, centrifuged and dialyzed until constant neutral pH in the effluent was achieved. CNC suspensions were then sonicated (Sonifier 450, Branson Ultrasonics, Danbury, CT) and placed over acidic cation exchange resin (Sigma-Aldrich, Milwaukee, WI). The final suspension was ca. 1 wt. % cellulose in water with a pH of 2.8 and was used in its acid form. The sulfuric acid hydrolysis reaction introduces sulfate half esters ($–OSO_3^-$) onto the surface of the CNCs, and the anionic surface charge density was measured to be 0.31 ± 0.04 e/nm^2 by conductometric titration with 0.01 M NaOH based on average crystal dimensions of 133 nm × 5 nm from TEM images. CNC suspensions were then concentrated by evaporation under ambient conditions and weight-percent concentrations of the final suspensions were measured by gravimetric analysis.

3.3.2 Modifications of Cellulose Nanocrystals

Aldehyde-Modified CNC Synthesis (CHO-CNC). 0.3 g of $NaIO_4$ was dissolved in 50 mL of a 1 wt. % CNC aqueous suspension. The mixture was allowed to stir for 2 h at room temperature before 0.15 mL of ethylene glycol was added quickly to the suspension.

The suspension was dialyzed as described above, and stored in suspension format at 4 °C. To obtain CHO-CNC with different degrees of functionality, the reaction time was set with 0.5 h and 24 h ending up with low-CHO-CNC and high-CHO-CNC.

Hydrazide-Modified CNC Synthesis ($NHNH_2$-CNC). 0.6 g of ADH was dissolved in 200 mL of a 1 wt. % COOH-CNC aqueous suspension. 0.014 g of NHS was suspended in 1 mL of a 1:1 DMSO:H_2O solution. 0.06 g of EDC was dissolved in 1 mL of a 1:1 DMSO:H_2O solution. NHS solutions and EDC solutions were added dropwise to the flask sequentially. The pH of the $NHNH_2$-CNC suspension was then adjusted to pH 6.8 using NaOH and HCl solutions until the pH of the solution no longer rapidly changed. The suspension was dialyzed as described above, and stored in suspension format at 4 °C.

3.4 Characterization of Components

Fourier Transform Infrared Spectroscopy (FTIR). FTIR spectra were recorded in transmission mode on a Nicolet 6700 FTIR spectrometer (Thermo Scientific) to qualitatively determine new functional groups by comparing the polysaccharides before and after modification. Lyophilized CMC-$NHNH_2$ and dextran-CHO were mixed with KBr powder and both mixtures were dried at 150 ^{o}C in the oven. For CNCs, CHO-CNCs or $NHNH_2$-CNC, KBr powder was added to the suspension, the mixture was well-stirred, and then dried at 120 ^{o}C in the oven. All the final powders were compressed into thin slices suitable for FTIR measurements. The results are shown in the Appendix A, Figures A.1-A.3.

Degree of Functionalization. The number of hydrazide groups on CMC-$NHNH_2$ or $NHNH_2$-CNCs was quantified by conductometric titration. For CMC-$NHNH_2$, the –COOH groups on CMC and CMC-$NHNH_2$ were titrated using 0.05 M NaOH to indirectly determine the amount of ADH that has reacted with CMC. Similarly, the –COOH groups on CNCs and $NHNH_2$-CNCs were titrated in the same method. The number of aldehyde groups on dextran-CHO or CHO-CNCs was determined by conductometric titration after selectively oxidizing the aldehyde groups to carboxylic acid groups using silver (I) oxide, as reported by Campbell *et al*. [80], [132]. Here dextran-CHO (0.05 g, ~0.0001 mmol) and NaOH (0.0248 g, 0.62 mmol) were dissolved in 10 mL of purified water, and silver (I) oxide (0.193 g) was added to the solution which was allowed to stir overnight. 5 mL of the oxidized reaction mixture was diluted with 80 mL of purified water and 0.85 mL of 1 M HCl. Finally, the solution was titrated using 0.05 M NaOH. A similar procedure was used for CHO-CNCs and a representative titration curve is shown in the Appendix A, Figure A.4.

Transmission Electron Microscopy (TEM). A JEM-1200EX TEM (JEOL Ltd., Japan) was used to image individual CNCs, CHO-CNCs or $NHNH_2$-CNCs at an acceleration voltage of 80 kV. For individual nanoparticle imaging, one drop of CNC suspension (0.001 wt. %) was placed onto a Formvar coated 200-mesh TEM grid (Canemco Inc., Canada), air dried, and stained using 2 wt. % uranyl acetate (Canemco Inc., Canada) for 1 min before removing the remaining liquid by absorption with filter paper.

3.5 Preparation of Injectable Hydrogels

A double-barrel syringe was used to make injectable hydrogels of chemically cross-linked CMC, dextran and CNCs. Barrel A contained a 4 wt. % CMC-$NHNH_2$ solution in purified water and barrel B contained a 4 wt. % dextran-CHO solution in purified water. To make CNC and CHO-CNC-reinforced hydrogels, barrel B also contained 0.1–2.0 wt. % of CNCs or CHO-CNCs. The final hydrogel was comprised of 2 wt. % CMC-$NHNH_2$, 2 wt. % dextran-CHO and 0.05–1.0 wt. % of CNCs or CHO-CNCs. CNCs in the dextran-CHO solutions were sonicated for 5 min before placing the suspensions in the syringe. The solutions/suspensions in barrel A and B were extruded through a static mixer placed at the outlet of the double-barrel syringe into a cylindrical rubber mold (9.5 mm in diameter × 1.5 mm in height) to prepare sample "disks" for analysis.

3.6 Characterization of Injectable Hydrogels

3.6.1 UV/Visible Spectroscopy

To test the stability of the dextran/CNC suspensions described above, turbidity (transmittance) was monitored over time for 4 wt. % dextran solutions with and without CNCs or CHO-CNCs. The turbidity of each suspension was measured at a wavelength of 450 nm using the Beckman Coulter DU® 800 UV/Visible spectrophotometer. The temperature was maintained at 25 ^{o}C during all measurements.

3.6.2 Rheology

Hydrogel rheology was studied following the procedure of Motlagh *et al*. [133] using an ARES rheometer (TA Instruments) with parallel-plate geometry. All the hydrogels were cylindrical with a diameter of 7 mm and a thickness of 1.5 mm. A dynamic frequency sweep test from 0.1 to 100 rad/s was taken to determine the dynamic storage modulus (*G'*) of each hydrogel, at a strain rate confirmed to be in the linear viscoelastic range for each type of hydrogel prepared. The temperature was maintained at 25 ^{o}C during all measurements. At least five different hydrogel disks were tested at each CNC loading concentration with the same experimental settings and average values are presented.

3.6.3 Swelling and Degradation

The swelling behavior of the hydrogels was measured in purified water and 10 mM phosphate buffered saline (PBS) solution at 37 °C. Hydrogels prepared using different concentrations of CNCs or CHO-CNCs with an initial weight (W_0) were immersed in a petri-dish with purified water or 10 mM PBS. The weight (W_x) was monitored over a period of 24 h. The swelling ratio was calculated using equation (1):

$$\text{Swelling Ratio (\%)} = 100 \times W_x/W_0 \qquad \text{Eq. (1)}$$

Hydrogel disks were also photographed over 60 days immersion in water and 10 mM PBS.

3.6.4 Morphology and Nano-Structure

Transmission Electron Microscopy (TEM). A JEM-1200EX TEM (JEOL Ltd., Japan) was used to image individual the injectable hydrogels at an acceleration voltage of 80 kV. For hydrogel imaging, samples were prepared to minimize the collapse of any inner pore structure. The hydrogels were solvent exchanged by immersing them in ethanol/H_2O solutions with increasing ethanol contents of 0%, 10%, 20%, 30%, 50%, 75%, 95% and 100%. Hydrogels were then embedded in Spurr's epoxy resin (Spurr 1969, Canemco Inc., Canada), fully dried, and cut into 80-100 nm thick transverse sections using an ultra-microtome. The sections were doubly stained with uranyl acetate and lead citrate (Canemco Inc., Canada) before imaging.

Scanning Electron Microscopy (SEM). A JEOL 7000F SEM (JEOL Ltd., Japan) was used to image hydrogels which had been carefully prepared to minimize collapse. Hydrogels were first solvent exchanged to ethanol as explained for TEM imaging and then critically dried in a critical point dryer. A scalpel was used to cut small sections of the hydrogels, which were subsequently sputtered with a 5 nm thick platinum coating before imaging.

3.6.5 *In Vitro* Cytotoxicity

The cytocompatibility of all the hydrogels as well as CNC and CHO-CNC suspensions was quantified using an MTT assay. NIH 3T3 fibroblasts were cultured in tissue culture flasks in DMEM supplemented with 10% FBS and 1% PS. All samples were sterilized

prior to testing and measurements were repeated four times, with error bars representing one standard deviation of the cell viability percentages measured.

The cytotoxicity of CNCs and CHO-CNCs was evaluated using an MTT assay over one day of material exposure. NIH 3T3 fibroblasts were plated at a density of 1.0×10^4 cells per well in a 24-well plate and maintained in DMEM media supplemented with 10% FBS and 1% PS. CNC and CHO-CNC suspension concentrations ranging from 100 to 1000 μg/mL were transferred into the wells with cultured cells and incubated for 24 h. Cell viability was characterized using a modified MTT assay, as described by Pawlikowska *et al*. [134], removing the CNC or CHO-CNC suspension, adding the MTT solution, and incubating over 4 h. The absorbance of the MTT solution was read using a Biorad microplate reader (model 550) at 570 nm against a 600 nm baseline and compared to that measured in cell-only wells in which no further materials were added. Cell viability was estimated according to equation (2):

$$\text{Cell viability (\%)} = \frac{\left(\text{absorbance}_{\text{test-exposed, 570 nm}} - \text{absorbance}_{\text{test-exposed, 600 nm}}\right)}{\left(\text{absorbance}_{\text{blank, 570 nm}} - \text{absorbance}_{\text{blank, 600 nm}}\right)} \qquad \text{Eq. (2)}$$

NIH 3T3 fibroblast cell cytocompatibility with the hydrogels (specifically, any leachates from the hydrogels) was assessed using a similar method. Hydrogels were made as previously described using the double-barrel syringe, injected into sterilized rubber cylindrical molds and then removed from molds after gelation (10 minutes). Cell viability was evaluated by seeding 2.0×10^4 cells per well under the cylindrical hydrogels in a 24-well plate and performing a 1-day MTT assay as previously described.

3.7 Preparation of Aerogels

1: Vortex Method. 5 mL of CHO-CNCs and 5 mL of $NHNH_2$-CNCs, in suspension at the same concentration (0.5, 1.0, 1.5 or 2.0 wt. %), were mixed in a 20 mL glass vial using a Vortex mixer for 2 min (Level 8, Analog Vortex Mixer, VWR, Canada). The hydrogels (mixtures) were transferred into a cylindrical glass vial (8 mm in diameter) and allowed to set for another 10 min before transfer into the freezer (-4 ^{o}C). After 12 hours, hydrogels were directly transferred into 100% ethanol at room temperature. Hydrogels were solvent exchanged to ethanol during the melting process without changing the size and shape. Finally, after changing the ethanol daily for 5 days, aerogels were obtained by drying in a critical point dryer.

2: Blending Method. A double-barrel syringe was used to make the chemically cross-linked aerogels. Barrel A and barrel B contained CHO-CNCs and CHO-CNCs, respectively, in suspension at identical concentrations (0.5, 1.0, 1.5 or 2.0 wt. %). The suspensions in barrel A and B were well mixed in the "blending area" of the double-barrel syringe and then were extruded out through the needle (tip 20G) into a cylindrical glass vial. The freezing, solvent exchange and critical point drying procedures are the same as described above for the Vortex Method.

3: Sonication Method. Aerogels prepared using the sonication method follow the "Vortex Method" procedure except that mixing the CHO-CNC and $NHNH_2$-CNC suspensions was performed under sonication for 5 or 15 min (35 kHz, 144W, Ultrasonic bath, VWR).

3.8 Characterization of Aerogels

3.8.1 Cross-Linking Ability of CHO-CNCs and $NHNH_2$-CNCs

Particle Size of Sol Suspensions. 0.5 wt. % of CHO-CNC and $NHNH_2$-CNC suspensions were mixed using the different mixing methods described. The particle size and distribution of each diluted suspension (0.1 wt. %) was measured using a Malvern Zetasizer Nano particle analyser. The temperature was maintained at 20 ^{o}C during all measurements.

Turbidity of Sol Suspensions. 0.5 wt. % of CHO-CNC and $NHNH_2$-CNC suspensions were mixed under Vortex for 2 min. The turbidity of each suspension (CHO-CNCs, $NHNH_2$-CNCs, supernatant of the mixture and lower turbid portion of the mixture) was measured at a wavelength of 450 nm using the Beckman Coulter DU® 800 UV/Visible spectrophotometer. The temperature was maintained at 25 ^{o}C during all measurements.

3.8.2 Density and Porosity

Density. Aerogel densities (ρ_{Gel}) were determined by measuring the weight and volume of each individual aerogel. The weight of an aerogel was measured by an analytical balance (readability 0.0001 g, Analystical Balance, Mettler Toledo) and the dimensions of an aerogel were measured by a digital caliper at four different positions. Five samples were used for density determination for aerogels with the same starting CNC concentration.

Porosity. Aerogel porosities (P) were calculated using the density of the aerogel (ρ_{Gel}) and density of cellulose nanocrystals (ρ_{CNC}) using equation (1), obtained from the simple rule of mixtures and assuming the gas density was negligible.

$$P\ (\%) = 100 \times (1 - \rho_{Gel} / \rho_{CNC}) \quad \text{Eq. (3)}$$

3.8.3 Brunauer–Emmett–Teller (BET) Analysis

The BET surface area was determined by N_2 adsorption and desorption using a Micrometric ADAP 2020 automated system (Micromeritics, USA). A sample was first degassed at 115 ^{o}C for 4 h prior to the analysis followed by BET analysis at -196 ^{o}C. The BET surface area and the Barrett-Joyner-Halenda (BJH) pore size distribution were calculated from the obtained isotherms.

3.8.4 Morphology and Nano-Structure

Morphology and Nano-structure. A JEOL 7000F SEM (JEOL Ltd., Japan) was used to image aerogels. Aerogels were immersed in liquid nitrogen and fractured to image the inner sections. A 5 nm thick platinum coating was applied before SEM imaging.

3.8.5 Mechanical Properties and Shape Memory Ability

Aerogels with different CNC contents were tested using a compress and release routine on a Mach-1Mechanical Testing System (Biomomentum, Canada). Each aerogel was made into a cylinder shape with a diameter of 8 mm and a height of 10 mm. The tests were carried out either in open-air or purified water, the maximum compression strain (ε)

was set at 0.2, 0.4, 0.6, 0.8 or 0.85, the speed of compressing and releasing was set at 1 mm/s. The shape-memory ability was assessed by calculating the shape recovery percentage using equation (4), in which the original height (h_{org}) and final height (h_{fin}) were measured:

$$Shape\ Recovery\ Percentage\ (\%) = {}^{h_{fin}}\!/_{h_{org}} \times 100\% \qquad \text{Eq. (4)}$$

3.8.6 Absorption Capacity and Reusability

Liquid Absorption Capacity. To determine the liquid absorption capacity of the CNC aerogels, different solvents were used including water, ethanol, DMSO and dodecane. A 0.5 wt. % CNC aerogel was submerged in a given solvent for 1 min until the absorbance reach the maximum loading. The weight of the aerogels before (W_{before}) and after (W_{after}) solvent uptake were measured, and the absorption capacity was calculated according to equation (5):

$$Absorption\ capacity\ (g/g) = {}^{W_{after}}\!/_{W_{before}} \qquad \text{Eq. (5)}$$

Reusability. To check the reusability of aerogels as absorbents, two different methods were used: **(1) Compression:** The absorbed solvent was manually squeezed out by compressing the aerogels. **(2) Evaporation:** The solvent-saturated aerogel was removed from the solvent bath and dried in the fume hood until it reached the original dry weight. The weight of aerogels before solvent absorption, after absorption, and after removing the

solvent was measured. A minimum of four samples and 20 cycles were tested for each experiment.

Error Calculations. All error bars and error intervals shown are confidence intervals (Δx) calculated from the estimated small data set standard deviation (S_x) of repeat measurements (N), that is, $\Delta x = S_x \times \text{t-value}/(N)^{1/2}$, where the t-value is the Student's t-distribution at a confidence level of 95% for $N-1$ degrees of freedom for individual measurements (unless otherwise noted).

CHAPTER 4: CELLULOSE NANOCRYSTAL-REINFORCED CARBOXYMETHYL CELLULOSE AND DEXTRAN HYDROGELS

This chapter presents the first injectable hydrogels reinforced both physically and covalently with cellulose nanocrystals. No additional chemicals, changes in temperature, or processing are required for gelation to occur – hydrazone cross-links are formed when the functionalized hydrogel components come into contact under normal physiological conditions. The macroscopic physical properties and microscopic internal structure of the hydrogels with different loading concentrations of CNCs and CHO-CNCs are reported. Swelling tests show that the hydrogels maintain their structure over the course of 60 days and are thus suitable for longer-term applications. New cellular toxicity studies for CNCs, aldehyde-modified CNCs and the CNC-reinforced hydrogels are presented which support the potential application of these materials in a clinical context.

The content in Chapter 4 has previously been published, and is reproduced with permission from:

Yang, X., Bakaic, E., Hoare, T., Cranston, E. D. Injectable polysaccharide hydrogels reinforced with cellulose nanocrystals: morphology, rheology, degradation, and cytotoxicity. Biomacromolecules 14, 4447–55 (2013).

4.1 Characterization of Injectable Hydrogel Components

Unfilled polymeric hydrogels and CNC-reinforced hydrogels with hydrazone cross-links were successfully prepared by extruding hydrazide and aldehyde-modified polysaccharides through a double-barrel syringe, as shown schematically in Figure 4.1. These double-barrel syringe systems have been extensively reported for a variety of applications [79]–[81]. The viscosities of both CMC and dextran/CNCs solutions prior to mixing are very low and thus can be easily injected through a double barrel syringe with even a narrow gauge needle at the tip (30G); gelation occurs rapidly after the polymers have been mixed by covalent bond.

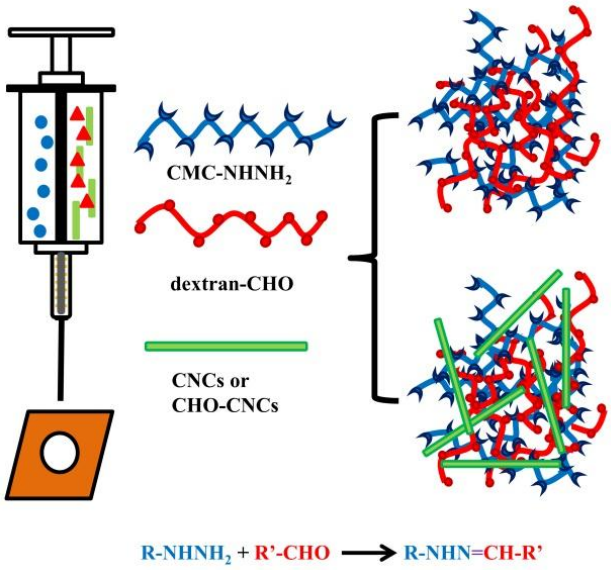

Figure 4.1. Schematic representation of injectable hydrogels reinforced with cellulose nanocrystals (CNCs), prepared using a double-barrel syringe. The cross-linking hydrogel components include hydrazide-functionalized carboxymethyl cellulose (CMC-$NHNH_2$), aldehyde-functionalized dextran (dextran-CHO) and either unmodified CNCs or aldehyde-modified CNCs (CHO-CNCs).

The degree of functionalization of the hydrogel precursor polymers was characterized by conductometric titration to determine the total number of potential cross-link sites (Table 4.1). For CMC-$NHNH_2$, 47 ± 8 % of the carboxyl groups on CMC were converted to hydrazide groups, corresponding to 2.6 ± 0.4 mmol of hydrazide groups per gram of CMC-$NHNH_2$. For dextran-CHO, 40 ± 6% of the ortho hydroxyl groups on dextran were oxidatively cleaved, resulting in 4.9 ± 0.7 mmol of aldehyde groups per gram of dextran-CHO. FTIR spectroscopy also supports the chemical functionalization of these polysaccharides as shown in Appendix A, Figures A.1 and A.2.

While unmodified CNCs were physically trapped between the chemically cross-linked CMC and dextran, the modified CHO-CNCs have the potential to react with CMC-$NHNH_2$ and thus be covalently cross-linked within the hydrogel. The number of aldehyde groups on each CHO-CNC was measured by selectively oxidizing the aldehyde groups to carboxyl groups with silver (I) oxide and titrating with NaOH (Appendix A, Figure A.4). We estimate that 12 ± 1% of CNCs' surface ortho hydroxyl groups have been oxidatively cleaved, resulting in ~2300 aldehyde groups per single CNC particle. The degree of functionalization per nanocrystal was calculated similar to a recent report [64], assuming CNCs are rectangular prisms and using the TEM dimensions determined herein with the X-ray diffraction unit cell coordinates of Nishiyama *et al.* [135]. FTIR spectroscopy (Appendix A, Figure A.3) and thermal gravimetric analysis (Appendix A, Figure A.5) of CNCs before and after modification further provide evidence for the addition of aldehyde groups to the CNCs.

Table 4.1. Dimensions and degree of functionalization of chemically-modified hydrogel components.

	CNC length × width* (nm)	**aldehyde groups (mmol/g)**	**hydrazide groups (mmol/g)**
CMC-$NHNH_2$	–	–	2.6 ± 0.4
dextran-CHO	–	4.9 ± 0.7	–
CNCs	133 × 5.0	–	–
CHO-CNCs	129 × 4.8	0.9 ± 0.1 (2300 ± 300 per CNC)	–

*Average length and width measured from TEM images for >100 individual CNCs, typical size distribution is 60-240 nm × 2-10 nm for CNCs and 60-220 nm × 2-9 nm for CHO-CNCs.

To incorporate nanoparticle reinforcement into the injectable hydrogels, CNCs were mixed with dextran-CHO and extruded in the same way as the unfilled hydrogels. Both CNCs and CHO-CNCs were easily dispersed and colloidally stable in dextran solutions over 30 days, as shown by negligible changes in turbidity measured by light transmittance (Figure 4.2). This implies that the two injectable hydrogel solutions, CMC-$NHNH_2$ and dextran-CHO with CNCs can be stored and remain unchanged over extended periods of time.

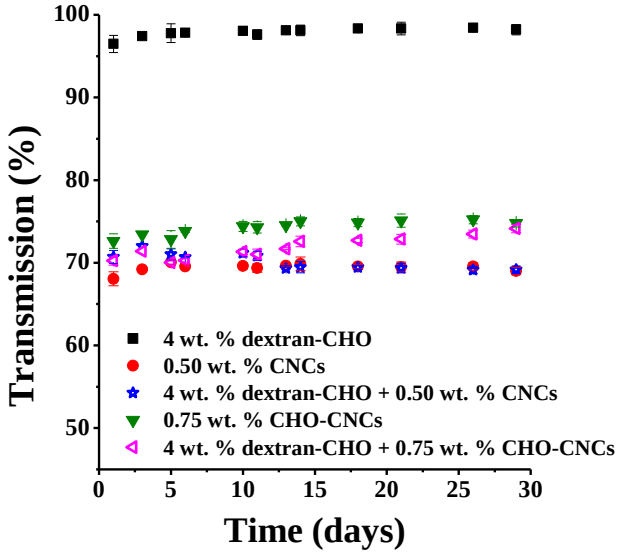

Figure 4.2. UV/Visible spectroscopy transmission (turbidity) of polymer solutions and CNC suspensions monitored over 30 days for 4 wt. % dextran solution with and without 0.5 wt. % CNCs or 0.75 wt. % CHO-CNCs. Confidence intervals are reported for $N = 4$ repeats with 95% confidence.

4.2 Appearance, Rheology and Mechanical Properties of Hydrogels

The effect of CNC loading and CNC surface chemistry on the appearance of the hydrogels and their mechanical properties was investigated. Each hydrogel was extruded into a disk-shaped mold (9.5 mm in diameter × 1.5 mm in height). Although the materials immediately formed a gel in all cases, the hydrogels were allowed to equilibrate for another 30 minutes before testing to ensure each sample was analyzed under comparable conditions. Visually, increasing the concentration of both CNCs and CHO-CNCs in the hydrogels resulted in a color change from transparent to opaque white, as shown in Figure 4.3. The decrease in transparency is not surprising, as CNC suspensions are also increasingly translucent with CNC concentration. Despite the color change, all hydrogels appeared visually uniform in density and color without any apparent

nanoparticle aggregation or caking. However, at much higher CNC loadings (ca. > 2 wt. %), gelation was noticeably hindered and the resulting hydrogels did include visible white particles (presumably agglomerated CNCs) within their structure.

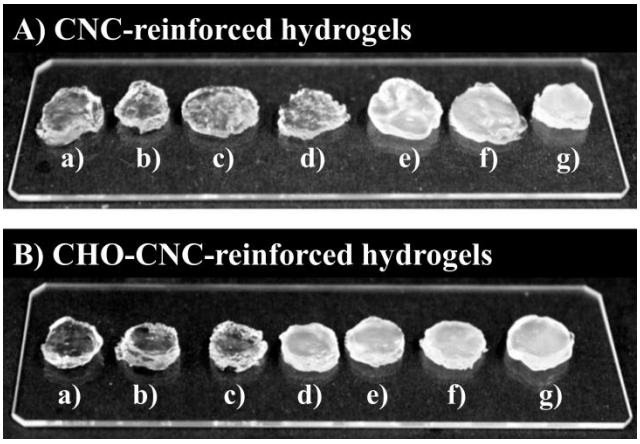

Figure 4.3. Photographs of reinforced injectable hydrogels (A) hydrogels with CNCs and (B) hydrogels with CHO-CNCs with loadings of a) 0, b) 0.05, c) 0.25, d) 0.375, e) 0.50, f) 0.75 and g) 1.0 wt. %.

Viscoelasticity of the injectable hydrogels was evaluated using parallel plate rheometry to measure the dynamic storage modulus (G') and the loss modulus (G'') which are shown in Figure 4.4. The G' values for all hydrogels were above 2000 Pa, while the G'' values for all hydrogels were below 800 Pa, over the full frequency range studied (Appendix A, Figures A.7 and A.8). As such, G' is much larger than G'' in all cases, indicating that the hydrogels are highly elastic. In fact, we can easily pick up the CNC-reinforced hydrogels by hand or using tweezers without inducing any obvious physical damage or flow in the gels.

The overall trend at low CNC loadings was for the storage modulus to increase relative to the unfilled hydrogels with increasing CNC concentration, followed by a

decrease in modulus above a critical CNC concentration (Figure 4.4). Likely, this is because at high loadings, the CNCs sterically block the cross-linking between dextran-CHO and CMC-$NHNH_2$. More specifically, the maximum G' for hydrogels with unmodified CNCs was 4100 Pa at 0.25 wt. % loading and the maximum G' for hydrogels with CHO-CNCs was 6700 Pa at 0.375 wt. % loading; or in relative terms, G' improved by 50 % by adding 0.25 wt. % of unmodified CNCs and by 140 % by adding 0.375 wt. % of CHO-CNCs. While the loadings that correspond to the maximum mechanical properties are relatively small, significant increases in storage modulus are achieved nonetheless, characteristic of large-aspect ratio nanoparticles [136]. The high crystallinity, Young's modulus and rigid rod shape of both types of CNCs lead to filled hydrogel networks with improved structural rigidity at low CNC concentrations.

The occurrence of a maximum modulus at low CNC loadings is generally consistent with previous work; however, a quantitative comparison to the literature is difficult because the hydrogel networks that were reinforced and the methods used to measure moduli and strength vary considerably [2]. For example, reinforcing α-cyclodextrin with 0.5 wt. % CNCs increased the storage modulus 50 times [95], but conversely, gelatin hydrogels required 17 wt. % of CNCs to achieve a maximum G' which was only a 150 % improvement over the unfilled gel [99]. Other hydrogel systems have used tensile strength and compression stress as a measure of enhanced mechanical properties; improvements of 150–300 % were observed at optimized loadings ranging from 1–7 wt. % CNCs [95], [98], [100], [127]. As such, our loading values that

correspond to maximum storage moduli are similar to other reports but with the advantage that our hydrogels are prepared from an injectable formulation.

Hydrogels with the aldehyde-modified CHO-CNCs had consistently larger storage moduli than the equivalent hydrogels with unmodified nanocrystals at the same loadings. This result is likely attributed to CHO-CNCs being both physically entrapped within, and chemically bound to, the hydrogel network. The ability to cross-link CHO-CNCs into the hydrogel led to improved mechanical properties overall and facilitated a higher maximum loading of nanoparticles prior to any observation of reduced G' values. For CHO-CNC loadings between 0.25 and 0.5 wt. %, the storage modulus was more than double that of the unfilled polymeric hydrogel. The peak G' for CHO-CNCs was 63 % higher than for the unmodified CNCs. All further characterization data presented is for CNC-reinforced hydrogels with the loadings that led to the highest storage modulus; however, the ability to tailor the mechanical strength by a factor of two by changing the CNC loading concentrations under 0.375 wt. % is noteworthy and implies potential applications for these hydrogels for tissue engineering of stiffer soft tissues (e.g. muscle) or as soft tissue adhesives. It should be noted that this elastic modulus matches that of neural and adipose tissue within the body, relevant to the successful use of such materials as cell scaffolds or delivery system *in vivo*. Soft tissue elasticity scales range from brain, fat, and striated muscle (0.1-10 kPa), and from stiff cartilage to pre-calcified bone (10-100 kPa) [137], [138].

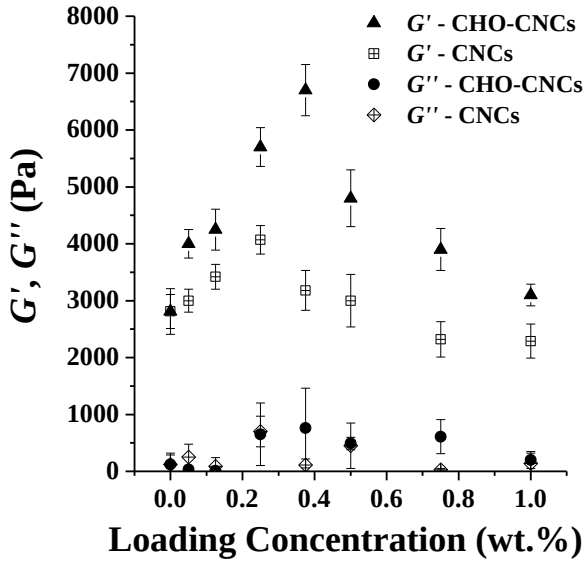

Figure 4.4. Dynamic storage modulus (G') and loss modulus (G'') of injectable hydrogels at different CNC or CHO-CNC loading concentrations, measured by parallel plate rheometry at a frequency of 75 rad/s. Confidence intervals are reported for N = 5 repeats with 95% confidence .

4.3 Swelling and Degradation of Hydrogels

Injectable hydrogels reinforced with CNCs were found to be more elastic and less swellable in solution relative to unfilled gels. Figure 4.5a shows swelling behavior, measured gravimetrically based on the increase in mass due to water uptake, in purified water at 37 ^{o}C over 24 h. After 24 h, swelling induced a mass increase of 310 ± 5 % in hydrogels without CNCs, while swelling of nanoparticle-reinforced hydrogels was restricted to 260 ± 5 % for CNC-containing hydrogels and 247 ± 4 % for CHO-CNC hydrogels. The swelling tests in 10 mM PBS show the same trends (Appendix A, Figure A.6). This phenomenon may be related to physical trapping and entanglement of the rigid CNCs within the dextran-CMC hydrogel which appears to reduce the mobility of the

polymer chains and/or may be due to the formation of hydrogen bonds between the CNC surfaces and the polymers, effectively increasing the cross-link density. The reduction in swelling is only slightly impacted when CNCs are also covalently cross-linked into the hydrogel, as seen for CHO-CNC-reinforced hydrogels. This result is consistent with previous work [100], [102] showing that the swelling ratio of hydrogels decreases as CNCs are more entangled or connected within the hydrogel network.

For applications in tissue engineering or long-term drug delivery, it is important to study the degradation of hydrogels over long time periods in addition to the swelling behavior. We monitored the shape and appearance of hydrogels over 60 days, and photographs tracking the changes are shown in Figure 4.5b. After swelling for 6 h, hydrogels with CNCs or CHO-CNCs maintain their structure better than unfilled polymeric hydrogels in accordance with the swelling data presented in Figure 4.5a. Even after 60 days in solution, the nanoparticle-reinforced hydrogels still remain in one piece, while the unfilled hydrogels degrade into fragments in a moderately viscous solution. Again, this observation implies that the CNCs and CHO-CNCs effectively reinforce the hydrogels to enable the gels to maintain their structure for a longer period of time compared to the control dextran-CMC hydrogels.

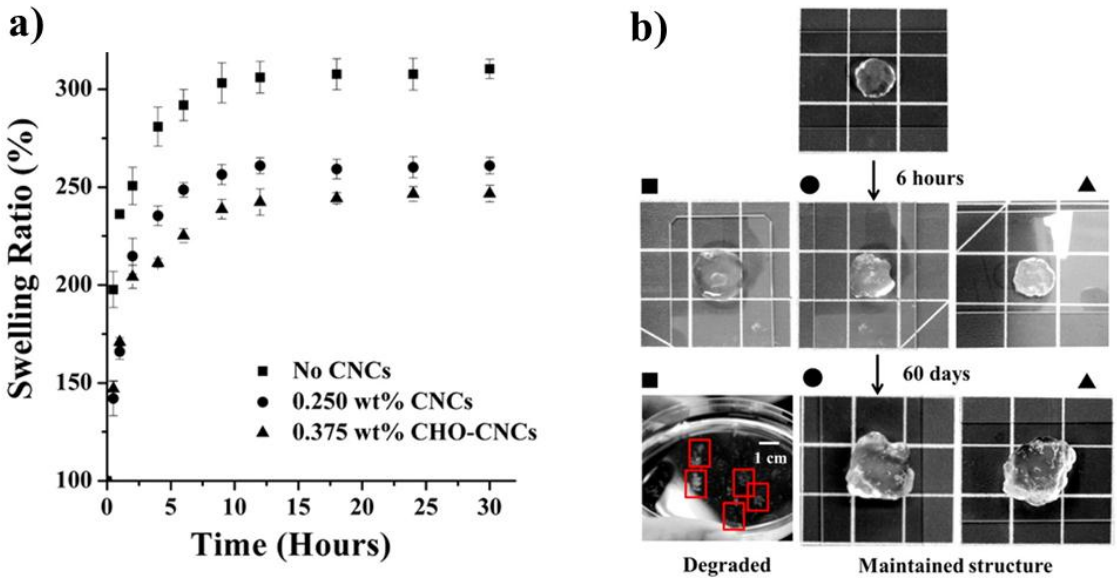

Figure 4.5. (a) Swelling of injectable hydrogels in purified water at 37 ^{o}C, confidence intervals are reported for N = 4 repeats with 95% confidence; (b) digital photographs of hydrogels with no CNCs (squares), CNCs (circles) and aldehyde-modified CNCs (triangles) after swelling for both 6 h and 60 days. (Background mat has 1 cm grid spacings and degraded hydrogel fragments are outlined with boxes).

4.4 Morphology of Hydrogels

The morphology, inner pore structure and uniformity of hydrogels play an important role in determining their potential applications. For example, pore size will dictate what type of drug can be entrapped (and the rate of that drug's release) from a hydrogel network while the roughness and molecular orientation in a hydrogel may aid in processes like cell differentiation in tissue engineering applications [139]. As shown in Figure 4.6, injectable hydrogels with and without CNCs had the same internal structure, showing a high density and uniform distribution of pores.

To try to capture the native (porous and highly hydrated) morphology of the hydrogels by SEM, samples were prepared by solvent exchanging to ethanol followed by

critical point drying, which is believed to minimize structural collapse [140], [141]. Pores visible by SEM are 60 to 90 nm in diameter which are slightly larger than the theoretically predicted pore size according to Paradossi *et al*. [142]. The calculated pore size is 30 nm for CMC and dextran hydrogels (having an interaction parameter of 0.563 and a characteristic ratio of 1.864) which is on the same order of magnitude as our pore sizes with the discrepancy likely related to sample preparation. Furthermore, we have only measured the clearly visible pores at this SEM magnification and this does not exclude the possibility of smaller sub-pores (which may be further masked by the Pt sputter-coated layer added for SEM imaging).

Both the pore size measured experimentally and the theoretical pore size for these injectable hydrogels are much smaller than those reported for other CNC-reinforced hydrogels, e.g., ~1 μm for α-cyclodextrin hydrogels [95], ~2 μm for gelatin hydrogels [99] and 10 μm for polyacrylamide hydrogels [100]. Overall, the uniformity and small pores observed in Figure 4.6 are unique to this work.

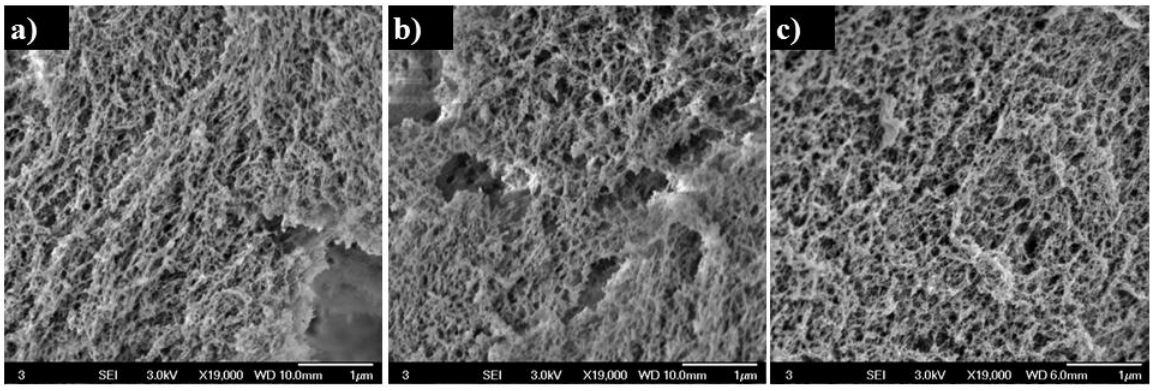

Figure 4.6. SEM images of hydrogels after critical point drying: (a) pure polymeric hydrogel with no CNCs, (b) CNC-reinforced hydrogel with 0.25 wt. % loading, (c) CHO-CNC-reinforced hydrogel with 0.375 wt. % loading.

CNC distribution and degree of agglomeration in the injectable hydrogels was assessed by imaging epoxy resin-embedded, ultra-microtomed hydrogel samples by TEM (Figures 4.7a, 4.7b and 4.7c). In all cases, individual cellulose nanocrystals are visible and well-distributed throughout the sample; uniform dispersion of CNCs in a reinforced composite is crucial to optimize the load-bearing ability of the nanoparticles and thus the mechanical properties of the hydrogel. This is the first report of single CNCs in a hydrogel being imaged.

In Figure 4.7, dextran and CMC polymers are more stained than cellulose nanocrystals and thus appear darker because the "stain-to-volume" ratio is higher for polymer chains than for CNCs. CNCs are only lightly stained on the outside due to their high crystallinity and general intractability. Nonetheless, the lighter-colored cellulose "needles" are also apparent, with some outlined with boxes in Figures 4.7b, 4.7c and 4.7d. Both CNCs and CHO-CNCs were well-dispersed and appear to be incorporated into the hydrogel network (shown magnified in Figure 4.7d). For comparison, CNCs and CHO-CNCs on a TEM grid are also shown in Figure 4.7e and Figure 4.7f, respectively. Some agglomeration between particles is seen due to drying aqueous CNC suspensions on TEM grids; however, only individual CNCs are observed in the hydrogels.

The tendency for CNCs to self-associate when dried or dispersed in most polymer matrices has notoriously limited their use in nanocomposites and led to mechanical

properties that fall short of theoretical predictions [3]. From the TEM images, the all-polysaccharide hydrogel developed herein appears to be an ideal matrix in which to disperse CNCs due to the chemical compatibility of the components and highly hydrated nature of the system, facilitating a high tolerance to the hydrophilicity and hydrogen-bonding proclivity of cellulose. Furthermore, a surprisingly uniform dispersion of CNCs in the hydrogel was achieved using the very simple "double-barrel syringe extrusion" procedure with polymer solutions in which CNCs remain stable for extended periods of time (Figure 4.2). Unlike other CNC-reinforced hydrogels which use strong mechanical stirring during the gelation to ensure the dispersion of CNCs [95], [99], [100], [102], this procedure only requires a short sonication treatment the first time that the CNC suspension and dextran-CHO solution are mixed.

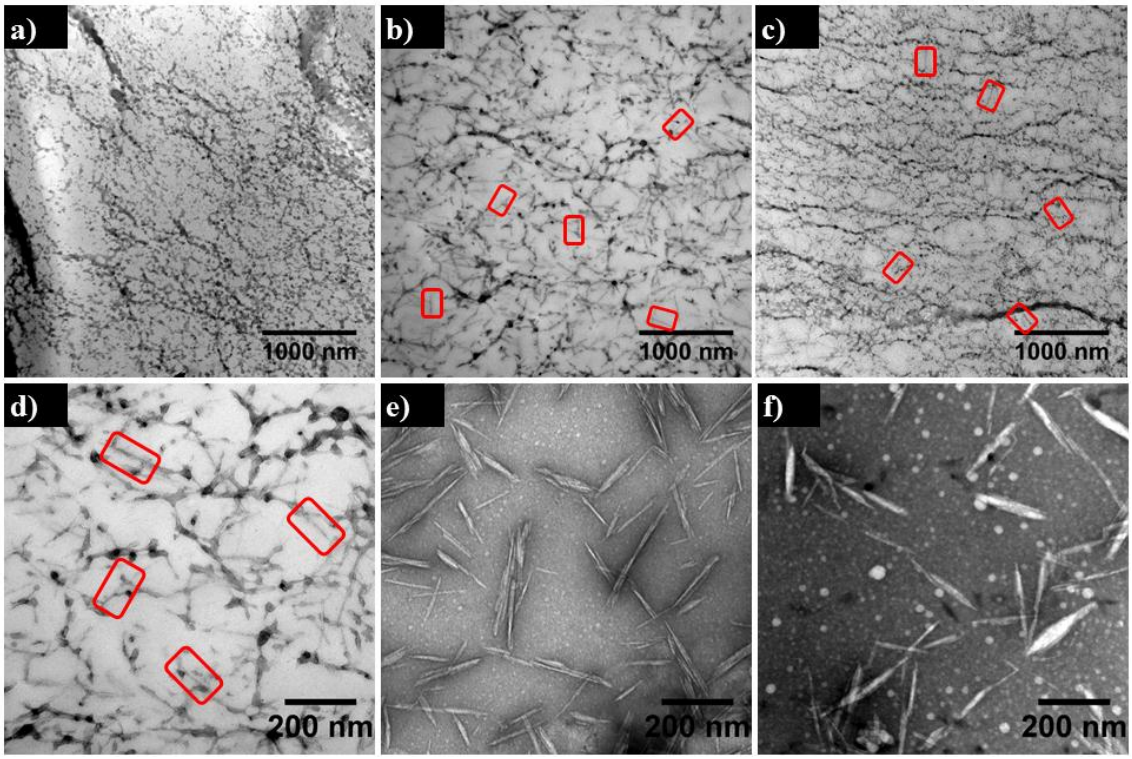

Figure 4.7. TEM images of stained 100 nm thick epoxy resin-embedded and ultra-microtomed hydrogels: (a) pure polymeric hydrogel with no CNCs, (b, d) CNC-reinforced hydrogel with 0.25 wt. % loading, (c) CHO-CNC-reinforced hydrogel with 0.375 wt. % loading; A few individual CNCs or CHO-CNCs are highlighted with red boxes. (e) TEM images of CNCs, (f) TEM images of CHO-CNCs.

4.5 *In Vitro* Cytotoxicity of Hydrogels

Preliminary *in vitro* cytotoxicity of CNC and CHO-CNC suspensions and hydrogels were assessed using an MTT assay with NIH 3T3 fibroblast cells. Figure 4.8 shows that all CNC suspensions (regardless of functionalization) induced only minimal decreases in relative cell viability over the concentration range of 100 to 1000 µg/mL after one day of cell exposure. Cytotoxicity of the gelled hydrogels (more specifically, any leachates from the hydrogels) was also tested by placing the molded hydrogels on top of the cells and performing a similar 1-day MTT assay. The results indicated that none of

the hydrogels exhibited significantly cytotoxicity; the relative viability of NIH 3T3 fibroblast cells was 0.93 ± 0.21 for unfilled hydrogels, 0.91 ± 0.16 for 0.25 wt. % CNC-reinforced hydrogels and 0.86 ± 0.16 for 0.375 wt. % CHO-CNC-reinforced hydrogels. (Confidence intervals are plus or minus one standard deviation.) This result indicates that the CNC and CHO-CNC-reinforced hydrogels may have potential for biomedical applications, although more thorough testing with human cell lines, as well as *in vivo* testing, would be required to confirm this potential [80], [81], [143].

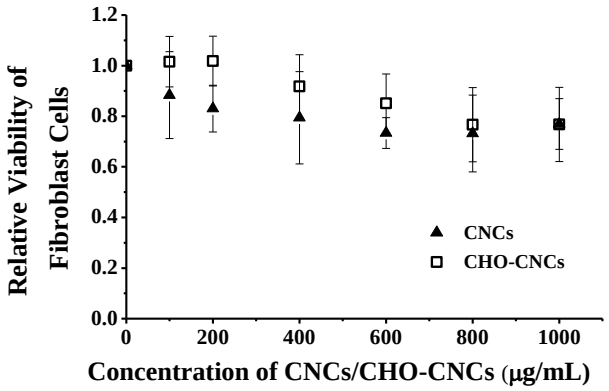

Figure 4.8. Relative viability (to cell-only control) of NIH 3T3 fibroblast cells for various concentrations of CNC (triangles) and CHO-CNC (squares) suspensions.

4.6 Conclusions and Future Work on Hydrogels

We have presented a new type of CNC-reinforced nanocomposite based on injectable polysaccharide hydrogels filled with CNCs that can act as simple fillers (unmodified CNCs) or as chemical cross-linkers (aldehyde-functionalized CNCs). The CNC-cross-linked hydrogels exhibited significantly higher elastic moduli (>140% increase at peak strength) relative to unfilled hydrogels without significantly impacting the pore structure of the hydrogels. We believe this result is due to the highly uniform

distribution of CNCs inside the hydrogels, as confirmed by SEM and TEM imaging, which is atypical for CNC nanocomposite materials. The CNC nanocomposite hydrogels also exhibited higher dimensional stability in extended (60 day) swelling experiments, remaining coherent while unfilled hydrogels degraded over the same time period. Both the starting components of the hydrogel, and the hydrogels themselves, showed no significant cytotoxicity to 3T3 fibroblasts in an MTT assay. Based on these results, CNC-reinforced injectable polysaccharide hydrogels are of potential interest in multiple biomedical applications, in particular, tissue engineering applications where longer term dimensional stability and/or enhanced mechanical strength are desirable.

In future work, further biocompatibility tests, including *in vivo* measurements, are needed if the materials are intended for biomedical applications. We may test CNCs' ability to reinforce other injectable hydrogel matrices to find the system most suitable for tissue growth studies. Another approach would be to replace the CNCs by NFC or BC, which have larger sizes and aspect ratios, and study the reinforcement. This will give us more information about how different nanocelluloses can reinforce highly cross-linked and entangled hydrogel materials.

CHAPTER 5: SHAPE-MEMORY CHEMICALLY CROSS-LINKED CELLULOSE NANOCRYSTAL AEROGELS

This chapter presents the first chemically cross-linked "all-CNC" aerogels, which have better mechanical properties due to using covalent bonds to form a networked structure instead of physical cross-linking. The density, porosity and microscopic internal structure of the aerogels with different starting CNC concentrations are presented. These ultralight, highly porous and flexible aerogels show superabsorbent capacities and shape-recovering abilities.

5.1 Characterization of Aerogel Components

The degree of functionalization of $NHNH_2$-CNCs and CHO-CNCs was characterized by conductometric titration to determine the total number of potential cross-link sites (Table 5.1). For $NHNH_2$-CNCs, 44 ± 7 % of the carboxyl groups on COOH-CNCs were converted to hydrazide groups, corresponding to 0.14 ± 0.02 mmol $NHNH_2$/g $NHNH_2$-CNCs. Aldehyde groups were generated by oxidation with sodium periodate resulting in CHO-CNCs with 0.9 ± 0.1 mmol CHO/g CHO-CNCs. FT-IR spectroscopy also supports the chemical functionalization of both modified CNCs, as shown in Appendix B, Figure B.1 and B.2.

Table 5.1. Dimensions and degree of functionalization of chemically-modified CNCs.

	length × width* (nm)	**aldehyde groups (mmol/g)**	**hydrazide groups (mmol/g)**
$NHNH_2$-CNCs	155 × 4.1	–	0.14 ± 0.02 (one group occupying ~7.4 nm^2)
CHO-CNCs	129 × 4.8	0.9 ± 0.1 (one group occupying ~1.2 nm^2)	–

*Average length and width measured from TEM images for >100 individual CNCs, typical size distribution is 100-260 nm × 2-7 nm for $NHNH_2$-CNCs, and 60-220 nm × 2-9 nm for CHO-CNCs.

5.2 Aerogel Formation

The chemically cross-linked "all-CNC" aerogels were successfully prepared following a simple sol-gel process consisting of mixing, freezing, solvent exchange and critical point drying without any initiator or additional chemicals/polymers. First, $NHNH_2$-CNC and CHO-CNC suspensions were mixed to form the initial sol whereby hydrazone cross-links form immediately upon mixing, creating small networked aggregates (Figure 5.1a). The sol suspension was then frozen to promote ice crystal growth (Figure 5.1b). The growing ice crystals push the cross-linked aggregates together to form a gel-like structure (Figure 5.1c) [94], [144], the ice crystals are removed through solvent exchange with ethanol and the final aerogel is obtained by critical point drying (Figure 5.1d).

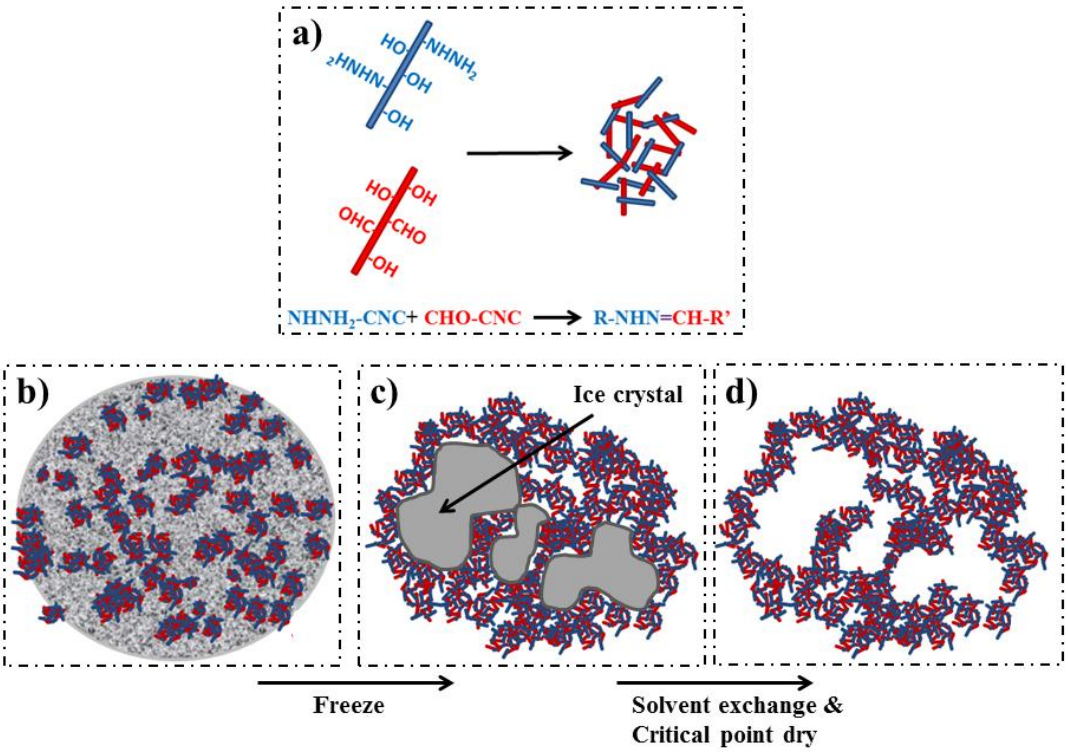

Figure 5.1. Schematic representation of chemically cross-linked CNC-only aerogels prepared by a sol-gel process: (a) formation of initial sols from $NHNH_2$-CNCs and CHO-CNCs, (b) sol suspension, (c) gel formation with the growth of ice crystal and (d) aerogel formation after solvent exchange with ethanol and critical point drying.

Different methods to mix the modified CNC suspensions were tested including Vortex mixing, sonication and double-barrel syringe blending. After freezing, however, the gel-like structures shrink substantially (>50%) or even disintegrate into pieces during the solvent exchange process for samples prepared by sonication or double-barrel syringe mixing. We believe that these mixing methods do not provide enough mixing for $NHNH_2$-CNCs and CHO-CNCs to form efficient aggregates, since the hydrazone cross-linking reaction needs the orthogonally-modified CNCs to come into close contact (sub-nanometer separations). We hypothesize that for CNCs at dilute concentrations (i.e., 0.5

wt. %), diffusion and light mixing is insufficient to bring enough particles into contact to form the large cross-linked aggregates required for robust aerogel formation.

DLS was used to track *apparent* particle and aggregate sizes of $NHNH_2$-CNCs, CHO-CNCs and mixtures from the three mixing methods. (The term *apparent* is used in recognition that this is a Z-average hydrodynamic diameter obtained from diffusion coefficients, assuming spherical particles, in a salt-free suspension and does not give absolute dimensions.) The results show that the aggregate size from sonication ranges from 150 to 3500 nm with a distribution peak at 185 nm with 81% intensity. The aggregate size from double-barrel syringe blending ranges from 160 to 2800 with a distribution peak at 213 nm with 83% intensity. Unmixed $NHNH_2$-CNC and CHO-CNC particle sizes are 141 nm and 135 nm, respectively; therefore most sol aggregates from these two mixing methods are small and only contain a few CNCs. On the contrary, the distribution peak of Vortex mixed samples is 1470 nm with 99.9% intensity, indicating that the aggregates are large and more uniform in size. Thus, the Vortex mixing method provides better mixing and allows for more efficient cross-linking, better gelation and a more extensive network structure in the final aerogel.

Interestingly, the sol suspension obtained through Vortex mixing, with aggregates ca. 1500 nm, is colloidally stable and does not show further aggregation or sedimentation over 1 month, as shown by negligible changes in turbidity (Appendix B, Figure B.3). TEM was used to image the structure of the modified CNCs (Figures 5.2a – 5.2b) and the sol suspensions (Figure 5.2c). The Vortexed mixture (Figure 5.2c) shows clear networks

formed by CNC particles, which imply successful cross-links. Without these cross-links, the mixture would appear more like $NHNH_2$-CNCs (Figure 5.2a) or CHO-CNCs (Figure 5.2b). All TEM samples were prepared from 0.0001 wt. % suspensions to avoid drying artefacts which could be confused with networked structures.

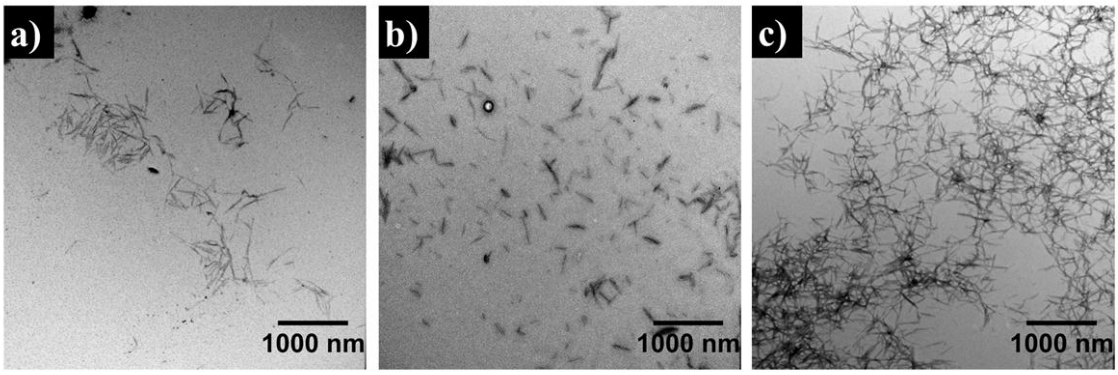

Figure 5.2. TEM images of dried suspensions: (a) $NHNH_2$-CNCs, (b) CHO-CNCs and (c) Vortexed mixture of orthogonally-functionalized CNCs.

5.3 Appearance, Density and Porosity of Aerogels

The effect of starting CNC concentration on the density and porosity of the final CNC aerogels was investigated. Figure 5.3a shows that the average density of aerogels ranges from 5.6 to 21.7 mg/cm^3 for aerogels prepared from 0.5 to 2.0 wt. % CNCs. These densities are significantly smaller than for previously reported "all-CNC" aerogels (78-155 mg/cm^3 from Heath *et al*. [126] and 22-31 mg/cm^3 from Dash *et al*. [127]). Figure 5.3b shows that the average porosity of aerogels decreases linearly with the starting CNC concentration from 99.6% to 98.6%. Lines in Figure 5.3 are theoretical predictions calculated using the theoretical density [145] and porosity and assuming no shrinkage during the solvent exchange and drying process. As such, we estimate that the shrinkage

of our aerogels is 11% which agrees with the reported range for nanocellulose aerogels (6.5 to 30% [126], [146]). It should be mentioned that our starting CNC concentration is only 0.5 to 2 wt. % which is much lower than for the work which reported shrinkage of 6.5% prepared from 8 wt. % NFC [126]. We believe that both the large modulus [2], [3] of highly crystalline cellulose nanocrystals and the strong cross-links from covalent bonds can significantly prevent shrinkage. Interestingly, the final ultralight aerogel can stand on top of a dandelion without bending the flower's hairs (Figure 5.3c).

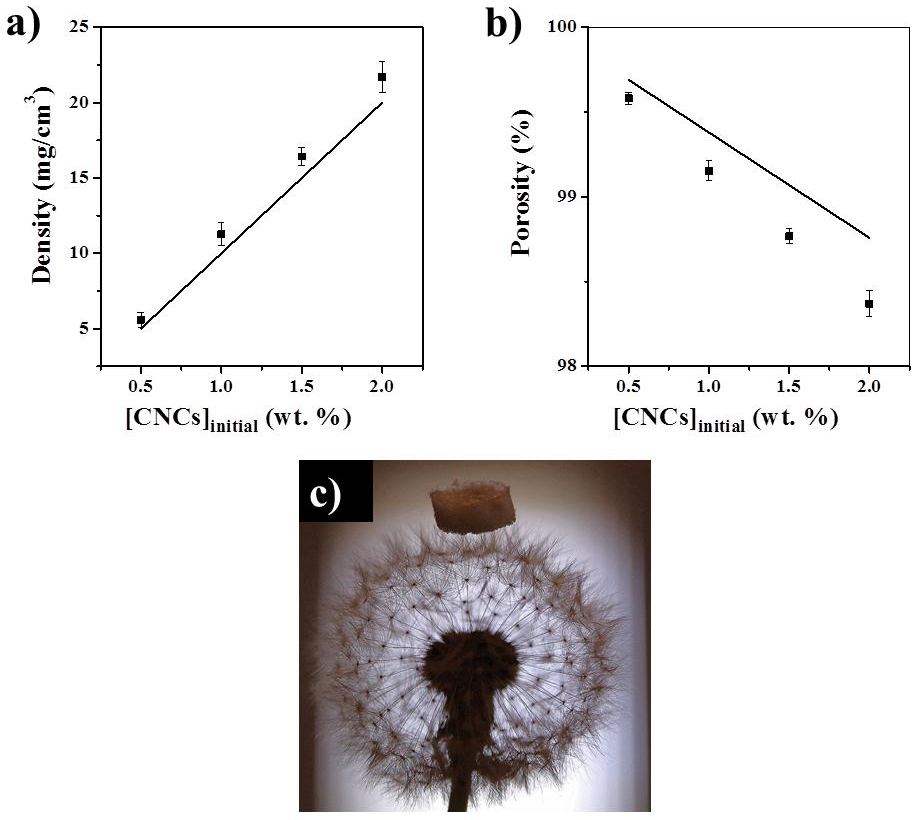

Figure 5.3. (a) Aerogel density and (b) porosity as a function of starting CNC concentration. The lines are theoretical predictions for no shrinkage during solvent exchange and drying. (c) Photo of a piece of CNC aerogel (prepared from 0.5 wt. % CNC suspension) standing on top of a dandelion.

5.4 Specific Surface Area and Pore Structure of Aerogels

The specific surface area of the CNC aerogels was determined by BET analysis to be 250 ± 80 m^2/g, which is in the range of that reported by Heath *et al*. (78-605 m^2/g) [126]. The surface area is theoretically calculated to be 512 m^2/g for individual CNCs under the assumption that length is 130 nm, width is 5 nm and density is 1.59 g/cm^3 [145]. The overlap of CNC particles due to cross-linking, and the sheet-like structures that result from freezing, will reduce the total specific surface area of the aerogels, making the measured value of 250 m^2/g reasonable.

We anticipated that our aerogels would have a bimodal pore distribution with micro or mesopores from CNC cross-links and macropores templated from ice crystal formation, as represented in Figure 5.1. BET analysis was used to determine the pore sizes for pores below 200 nm. CNC aerogels prepared from 0.5 wt. % CNC suspensions were found to have a mesoporous volume of 0.25 cm^3/g, while the total calculated pore volume is 178 cm^3/g. Thus mesopores make up ~0.14% of the total pores. As CNCs occupy only 0.4% of the total aerogel volume, and are responsible for the cross-link-generated mesopores, the overall mesopore volume is reasonable. As a comparison, mesopores constitute roughly 4-11% of the total porosity of the aerogels prepared by Heath *et al*. which is greater than in our aerogels, but they were using a much higher starting CNC concentration (8 to 16 wt. %) which dramatically reduces the overall pore volume [126].

Interestingly, the BJH pore size distribution (Figure 5.4) shows a single peak at 8 nm which indicates that our mesopores are uniform and small. Both chemical cross-linking between orthogonally-functionalized CNCs and the size uniformity of CNCs themselves are likely responsible for the uniform pore structure and minimal collapse of the aerogels during drying. In contrast, Heath *et al*. prepared physically cross-linked CNC aerogels which displayed two peaks at 4.3 and 15.5 nm [126], and they propose that further investigation is needed to understand the origin of the two pore sizes.

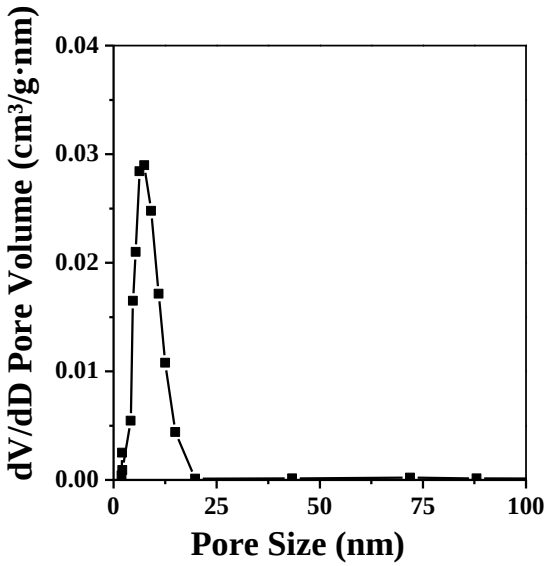

Figure 5.4. Mesopore size distribution in aerogels prepared from 0.5 wt. % starting CNC concentration from BJH analysis based on pore area.

5.5 Aerogel Morphology

SEM images of aerogels from different starting CNC concentrations clearly show the internal nano and micro-structure of the aerogels (Figure 5.5). All the aerogels exhibit a similar internal pore structure with bigger pores (>1 μm) and smaller pores (< 50 nm) as

expected from BET analysis and density/porosity measurements. Specifically, macropores are seen at low magnification (Figure 5.5, top), while the mesopores are seen by zooming in on the "walls" which form the macropores (Figure 5.5, bottom). The mesopore structure from CNC cross-links shows a promising 3D interconnected network, such that even though the macropores are not necessarily connected, water, gas or other small molecules can still pass through this porous aerogel "mesh". Additionally, the mesopore structure is consistent with the TEM images of the sol suspension (Figure 5.2). As the starting CNC concentration increases, aerogels tend to have more macropores with smaller sizes. However, the mesopore structure stays the same. We believe the mesopores are coming from the cross-links between CNC particles which are more or less independent of the starting CNC concentration. On the other hand, increasing the concentration of CNCs means CNCs occupy more space in the mixture and ice crystals will be smaller which results in smaller macropores when the ice crystals are removed.

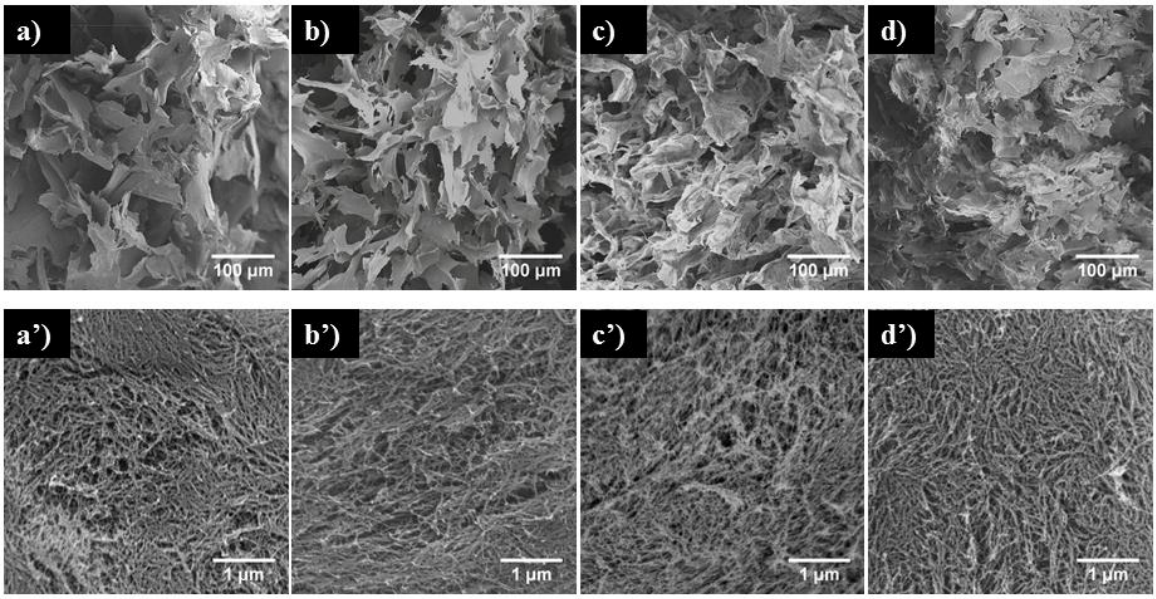

Figure 5.5. SEM images of aerogels with different starting CNC concentrations: (a, a') 0.5 wt. %, (b, b') 1.0 wt. %, (c, c') 1.5 wt. % and (d, d') 2.0 wt. %. Macropores are visible at low magnifications (top, a-d) and mesopore uniformity is observed at higher magnification (bottom, a'-d').

5.6 Mechanical Testing of Aerogels

The CNC aerogels are strong and remain intact when compressed in both air and liquid environments. Figure 5.6a shows the compressive stress-strain behaviour of aerogels in air, where three regions are apparent: a flat region of low stress (< 1.1 kPa) below 20% strain, a slowly increasing stress response between 20 and 80% strain, and an exponentially increasing stress response above 80% strain. At 80% strain, the compressive stress of CNC aerogels prepared from 0.5, 1.0, 1.5 and 2.0 wt. % CNCs is 8.9, 11.6, 15.7 and 20.5 kPa, respectively. This is similar to NFC aerogels of Jiang *et al.* [113] which exhibited a compressive stress of 8.5 kPa at 80% strain. Furthermore, at 95% strain, the compressive stress of each aerogel is 17.5, 26.8, 53.0 and 105.3 kPa. From

these results, we believe that aerogels from higher starting concentrations of CNCs will have a larger proportion of chemically cross-linked parts (i.e., more "solid-like" parts over hollow parts) and thus they will exhibit higher stress at the same compressive strain compared to aerogels prepared from low starting concentrations.

Figure 5.6b shows that water saturated CNC aerogels display excellent wet strength as well. The compressive stress is low below 80% strain, but monotonically increases from 80% to 95% strain. At 80% strain, the compressive stress of aerogels prepared from 0.5, 1.0, 1.5 and 2.0 wt. % CNCs is 0.8, 1.7, 2.2 and 3.7 kPa, respectively. These values are within range of some similar work, such as 1.2 kPa for NFC aerogels [113] and 12.1 kPa for carbon aerogels [147] which were compressed 80%. At 95% strain, the compressive stress of each aerogel is 15.2, 26.6, 30.7 and 44.4 kPa which is more than 10 times larger than the stress at 80% strain.

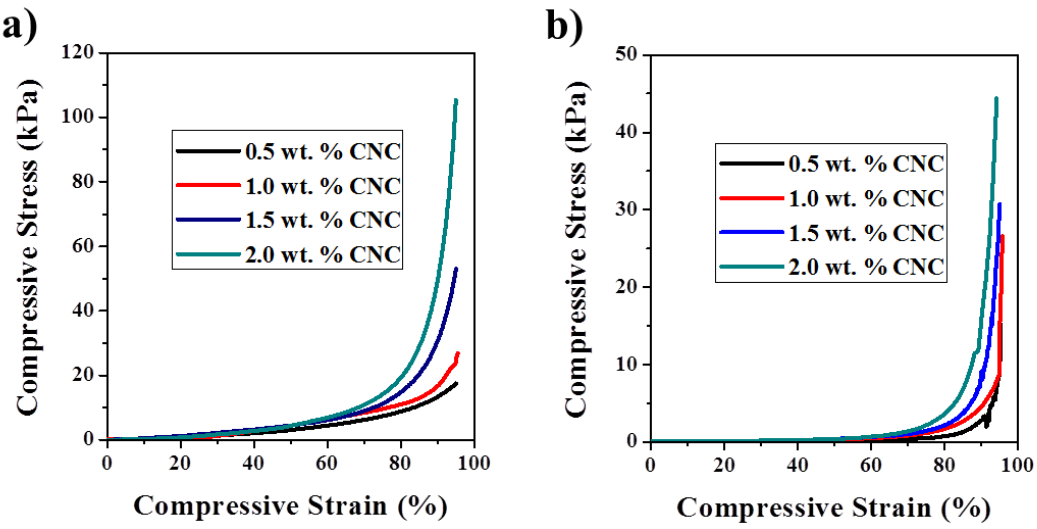

Figure 5.6. Compressive stress-strain curves of aerogels prepared from 0.5, 1.0, 1.5 and 2.0 wt. % CNC suspensions, from 0 to 95% strain in (a) air and (b) water.

The compressive stress of aerogels in water (i.e., aerogels reconstituted into hydrogels) is much lower than in air, since the water acts as a plasticizer and softens the hydrogel by forming hydrogen bonds between water molecules and CNCs, and disrupts some CNC-CNC hydrogen bonding [148]. In polar solvents, the decrease in cellulose-cellulose interactions will make the aerogels less robust. This also supports the observation that stress is greater at low strain for dry aerogels, whereas the hydrogels have a flat stress dependence until 80% strain. Combining the morphological characterization and the mechanical measurements of these aerogels, it appears that the macropores are compressed first, whereby the resistance to compression stems mainly from hydrogen bonds and physical cross-links, and then the chemically cross-linked CNC networks are compressed or broken at higher strains.

Cyclic compression tests were undertaken to determine the shape-recovering ability of aerogels after 20 cycles. Figure 5.7a shows that all the CNC aerogels in air can return to ~90% of their original height after being compressed 20%, but the shape recovery percentage decreases with increasing compressive strain. Above 95% strain in air, the aerogels cannot easily recover their original shape. On the contrary, Figure 5.7b shows that all CNC aerogels in water will recover at least 85% of their original size, and furthermore, the shape recovery percentage is above 50%, even at 95% strain. Specifically, the aerogels from 0.5 wt. % CNC suspensions can recover 85% of their original size after 95% compression which has not been shown previously for other nanocellulose aerogels. In fact, the literature shows that aerogels are generally not tested

above 80% strain and show inferior shape recovery abilities even at these relatively low compressions [113],[147].

The cyclic compression tests (Figure 5.7) are consistent with the compressive stress-strain curves (Figure 5.6): the aerogels recover to their original height if compressive stress does not exceed the flat region of the stress-strain curve, i.e., when the chemical cross-links are not broken. It is also noteworthy that the recovery speed of aerogels in water is ~1 mm/s and the aerogels can return to their original height from 95% compression in under 11 seconds. This recovery is similar to NFC aerogels of Zhang *et al*. [149]. We believe that the unique pore structure in our cross-linked CNC aerogels aid in fast shape-recovery; the mesopores absorb the water quickly due to capillary action and the macropores store and transfer the water.

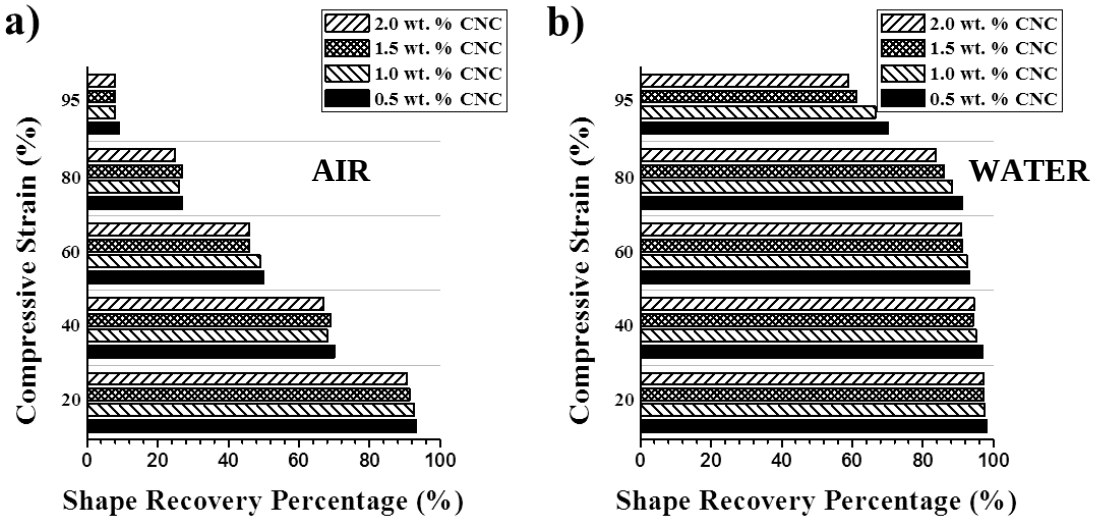

Figure 5.7. Shape recovery percentage of aerogels prepared from 0.5, 1.0, 1.5 and 2.0 wt. % CNC suspensions under different compressive strains after 20 cyclic compressions: (a) in air and (b) in water.

5.7 Absorption Capacity of Aerogels

Cellulose has an abundance of hydroxyl groups in its chemical structure which leads to an overall affinity for water and other polar liquids. CNC aerogels made from 0.5 wt. % CNC suspensions were used to determine the absorption capacity of aerogels in various solvents. This sample was chosen since it has the highest porosity and the best shape-recovering ability. Figure 5.8 shows that 160 ± 10 g of water, 130 ± 10 g of ethanol or 134 ± 8 g of DMSO can be absorbed per gram of aerogel (on the first absorption cycle). Based on the calculated pore volume of 178 cm^3/g, about 87%, 89% and 68% of the pores are filled with these three solvents, respectively. Interestingly, 72 ± 5 g of dodecane (a hydrophobic oil) can also be absorbed, filling about 54% of the total pore volume. We believe that the capillary forces imparted by the mesopores of the aerogels help with the absorption of dodecane yet the larger pores are not fully filled because CNCs and dodecane are incompatible based on their surface energy. It takes less than 10 seconds for the aerogels to absorb the solvents tested to their maximum loading. This ultra-fast absorbing quality is another unique feature of our aerogels.

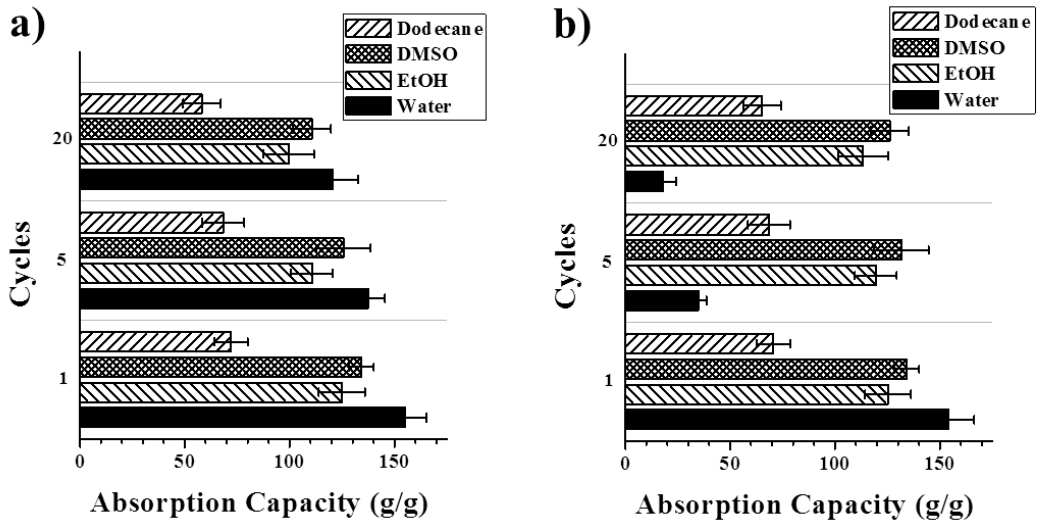

Figure 5.8. Cyclic absorption capacity of aerogels prepared from 0.5 wt. % CNC suspensions for different solvents using different desorbing methods: (a) squishing the solvent out and (b) letting the solvent evaporate.

Cyclic absorption capacity was tested to check the reusability of aerogels made from 0.5 wt. % CNC suspensions. Two desorbing methods were used: squishing the solvent out (Figure 5.8a) and letting the solvent evaporate (Figure 5.8b). By using the former method, the absorption capacity of aerogels slightly decreases which is consistent with the shape-recovery tests. More precisely, the absorption capacity of aerogels decreases from 155 to 121 for water, 125 to 100 for ethanol, 134 to 111 for DMSO and 72 to 58 for dodecane (absorption capacity values are reported as g of solvent per g of aerogel). By the evaporation method, the absorption capacity of aerogels is very similar in ethanol, DMSO and dodecane, however, this is not the case for water. Water is not easily evaporated from the aerogels under ambient conditions and the absorption capacity decreases significantly from 155 to 18, on the 20^{th} cycle. Strong hydrogen bonding of water to cellulosic materials is well known and furthermore, the hydration of the aerogels

to hydrogels likely results in a rearrangement of the network gel structure, a loss of the larger pores and an internal collapse of the structure overall. Ethanol, DMSO and dodecane appear to have less ability to disrupt the original aerogel structure and hydrogen bonding overall.

Interestingly, the absorption preferences of CNC aerogels may give them the ability to separate oil and water. Figure 5.9 shows a series of images of aerogels picking up water from a dodecane/water mixture, where water is denser and sits at the bottom of the vial. As an aerogel is immersed into the vial, it first absorbs dodecane, however, as it comes into contact with water, the dodecane is displaced (in under 1 second) and the water-filled aerogel can be removed from the vial.

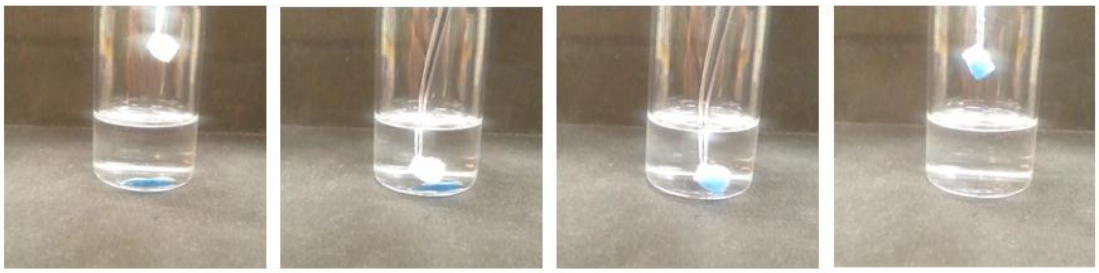

Figure 5.9. Chronological photographs of an aerogel picking up water from a dodecane/water mixture. Water is been dyed with blue color for easier visualization.

5.8 Conclusions and Future Work on Aerogels

We have presented a new type of chemically cross-linked "all-CNC" aerogels based on hydrazone cross-links between $NHNH_2$-CNCs and CHO-CNCs. The final aerogel shows ultralight weight (5.6 to 21.7 mg/cm^3), and high porosity (99.6% to 98.6%). This CNC aerogel displays bimodal pore distribution (mesopores ~8 nm and

macropores >1 μm), as confirmed by BET analysis and SEM. We believe the mesopores are coming from the CNC cross-links and macropores are coming from ice templates. These CNC aerogels shows great mechanical properties and shape-recovering abilities, especially in water (recovers at least 85% of its shape at 80% strain after 20 compress and release cycles). These CNC aerogels also show great absorbency of both water (160 ± 10 g per g) and dodecane (72 ± 5 g per g), and cyclic absorption capacities are maintained even after 20 cycles. Based on these results, these chemically cross-linked "all-CNC" aerogels have potential applications as superabsorbent and in oil/water separations.

In future work, it may be worth studying how the degree of functionalization (of CHO and $NHNH_2$ groups) will affect the cross-linking density and pore structure in CNC hydrogels and aerogels. The robust aerogels presented here may lend themselves well to application as substrates which can be back-filled with other polymers to create polymer nanocomposites, or even porous polymer materials obtained by removing the CNCs. Additionally, we plan to use this CNC aerogel, and similar cross-linked CNC films, as a substrate to grow metal–organic framework (MOF) membranes (in collaboration with He Zhu, PhD student with Dr. Zhu, McMaster University). The desired result is a porous aerogel totally covered by a MOF membrane which may be useful for gas separations.

CHAPTER 6: CONCLUSIONS AND RECOMMENDATIONS

Creating new functional materials using nanotechnology and renewable components has become a popular research area. With advantages like low cost, biocompatibility, biodegradability, good mechanical properties and chemically reactive surfaces, cellulose nanocrystals make up a promising class of nanomaterials which have potential applications spanning food, personal care, biomedical devices, textiles, separation technologies, construction materials as well as more traditional paper and board products.

In this thesis, we have presented the use of chemically cross-linkable cellulose nanocrystals as (1) nano-fillers to reinforce injectable hydrogels and (2) nano-fibers to generate "all-CNC" aerogels. Taking advantage of CNCs' unique properties such as large aspect ratio, high strength and light weight, together with the chemical cross-linking ability of modified CNCs, the final injectable hydrogels and aerogels have impressive mechanical properties.

In the injectable hydrogel section (Chapter 4), we have presented a new type of CNC-reinforced nanocomposite based on injectable polysaccharide hydrogels filled with aldehyde-functionalized CNCs which act as both nano-fillers and cross-linkers. The final hydrogel exhibited significantly higher elastic moduli (>140% increase at peak strength) and higher dimensional stability over long term swelling experiments, remaining coherent while unfilled hydrogels degraded over the same time period. Additionally, the final hydrogel showed no significant cytotoxicity to 3T3 fibroblasts in an MTT assay. All these

results support that our hydrogels may be used in biomedical applications, in particular, in tissue engineering applications where longer term dimensional stability and/or improved mechanical strength are desirable.

In the aerogel section (Chapter 5), we have presented a new type of chemically cross-linked "all-CNC" aerogel based on hydrazone cross-linking between $NHNH_2$-CNCs and CHO-CNCs. These ultralight and highly-porous aerogels exhibited great mechanical properties and shape recovering ability, especially in water. These CNC aerogels also showed superabsorbent tendencies with both water and dodecane, and the cyclic absorption capacity was maintained even after 20 cycles. These properties make the chemically cross-linked CNC aerogels suitable for applications such as absorbents for different solvents or for separation technologies.

The introduction of cross-linkable functional groups onto the surface of CNC particles allows for CNCs to be covalently bound into a polymer matrix or to be cross-linked to each other. Gel nanomaterials based on chemically cross-linked CNCs have shown greater mechanical properties than for physically cross-linked gels, or materials which rely on hydrogen bonding alone to create a networked internal structure. Our work focuses on hydrazone cross-link chemistry because it is a fast and easy gelation process, however, other cross-linking chemistries may be used as well, and may bring about other advantages. There are always challenges regarding how to tune the surface chemistry of CNCs to make them compatible with surrounding materials and/or suitable for various

applications; this work is one step towards tailored nanomaterials that take advantage of modified CNCs which can impart new or enhanced properties to the final products.

References

[1] A. Dufresne, *Nanocellulose: From Nature to High Performance Tailored Materials*. Walter De Gruyter Inc, Berlin, 2012.

[2] R. J. Moon, A. Martini, J. Nairn, J. Simonsen, and J. Youngblood, "Cellulose nanomaterials review: structure, properties and nanocomposites", *Chem. Soc. Rev.*, vol. 40, no. 7, pp. 3941–3994, 2011.

[3] Y. Habibi, L. A. Lucia, and O. J. Rojas, "Cellulose Nanocrystals: Chemistry, Self-Assembly, and Applications", *Chem. Rev.*, vol. 110, no. 6, pp. 3479–3500, 2010.

[4] S. Kalia, B. S. Kaith, and I. Kaur, *Cellulose Fibers: Bio- and Nano-Polymer Composites: Green Chemistry and Technology*. Springer, Berlin, 2011.

[5] Future Markets, *The global market for nanocellulose to 2020*, 2nd ed. Future Markets Inc, 2012.

[6] M. Mariano, N. El Kissi, and A. Dufresne, "Cellulose nanocrystals and related nanocomposites: Review of some properties and challenges", *J. Polym. Sci. Part B Polym. Phys.*, vol. 52, no. 12, pp. 791–806, 2014.

[7] M. A. S. Azizi Samir, F. Alloin, and A. Dufresne, "Review of Recent Research into Cellulosic Whiskers, Their Properties and Their Application in Nanocomposite Field", *Biomacromolecules*, vol. 6, no. 2, pp. 612–626, 2005.

[8] E. Doelker, "Cellulose derivative", in *Biopolymers I*, R. Peppas and N. Peppas, Eds. Springer, Berlin, 1993.

[9] D. M. Updegraff, "Semimicro determination of cellulose in biological materials", *Anal. Biochem.*, vol. 32, no. 3, pp. 420–4, 1969.

[10] B. L. Peng, N. Dhar, H. L. Liu, and K. C. Tam, "Chemistry and applications of nanocrystalline cellulose and its derivatives: A nanotechnology perspective", *Can. J. Chem. Eng.*, vol. 89, no. 5, pp. 1191–1206, 2011.

[11] *McGraw-Hill Yearbook of Science And Technology 2008 (Mcgraw Hill Yearbook of Science & Technology)*. McGraw-Hill Professional, New York, pp. 225–228, 2008.

[12] S. J. Eichhorn, "Cellulose nanowhiskers: promising materials for advanced applications", *Soft Matter*, vol. 7, no. 2, pp. 303–315, 2011.

[13] G. Chinga-Carrasco, “Cellulose fibres, nanofibrils and microfibrils: The morphological sequence of MFC components from a plant physiology and fibre technology point of view”, *Nanoscale Res. Lett.*, vol. 6, no. 1, p. 417, 2011.

[14] S. Beck-Candanedo, M. Roman, and D. G. Gray, “Effect of Reaction Conditions on the Properties and Behavior of Wood Cellulose Nanocrystal Suspensions”, *Biomacromolecules*, vol. 6, no. 2, pp. 1048–1054, 2005.

[15] R. M. Brown Jr, “The biosynthesis of cellulose”, *Food Hydrocoll.*, vol. 1, no. 5–6, pp. 345–351, 1987.

[16] D. P. Delmer and Y. Amor, “Cellulose biosynthesis”, *Plant Cell*, vol. 7, no. 7, pp. 987–1000, 1995.

[17] A. Cavka, X. Guo, S.-J. Tang, S. Winestrand, L. J. Jönsson, and F. Hong, “Production of bacterial cellulose and enzyme from waste fiber sludge”, *Biotechnol. Biofuels*, vol. 6, no. 1, p. 25, 2013.

[18] M. E. Malainine, A. Dufresne, D. Dupeyre, M. Mahrouz, R. Vuong, and M. R. Vignon, “Structure and morphology of cladodes and spines of Opuntia ficus-indica. Cellulose extraction and characterisation”, *Carbohydr. Polym.*, vol. 51, no. 1, pp. 77–83, 2003.

[19] Y. Habibi, A.-L. Goffin, N. Schiltz, E. Duquesne, P. Dubois, and A. Dufresne, “Bionanocomposites based on poly([varepsilon]-caprolactone)-grafted cellulose nanocrystals by ring-opening polymerization”, *J. Mater. Chem.*, vol. 18, no. 41, pp. 5002–5010, 2008.

[20] A. N. Nakagaito, S. Iwamoto, and H. Yano, “Bacterial cellulose: the ultimate nano-scalar cellulose morphology for the production of high-strength composites”, *Appl. Phys. A*, vol. 80, no. 1, pp. 93–97, 2005.

[21] J. Simonsen, “Bio-based nanocomposties: challenges and opportunities.” [Online]. Available: http://people.forestry.oregonstate.edu/john-simonsen/sites/devel-d7.forestry.oregonstate.edu.john-simonsen/files/Nanocomposites.pdf. [Accessed: 05-June-2014]

[22] M. Matus, “Super-Durable Material Made from Wood Waste is Stronger, Cheaper, and Lighter Than Kevlar”, 2012. [Online]. Available: http://inhabitat.com/super-durable-material-made-from-wood-waste-is-stronger-cheaper-and-lighter-than-kevlar/. [Accessed: 05-June-2014]

[23] M. C. B. de Figueirêdo, M. de F. Rosa, C. M. L. Ugaya, M. de S. M. de Souza Filho, A. C. C. da Silva Braid, and L. F. L. de Melo, "Life cycle assessment of cellulose nanowhiskers", *J. Clean. Prod.*, vol. 35, no. 0, pp. 130–139, 2012.

[24] S. Dong, A. Hirani, K. R. Colacino, Y. W. O. O. Lee, and M. Roman, "Cytotoxicity and Cellular Uptake of Cellulose Nanocrystals", *Nano Life*, vol. 02, no. 03, p. 1241006, 2012.

[25] S. Montanari, M. Roumani, L. Heux, and M. R. Vignon, "Topochemistry of Carboxylated Cellulose Nanocrystals Resulting from TEMPO-Mediated Oxidation", *Macromolecules*, vol. 38, no. 5, pp. 1665–1671, 2005.

[26] T. Kovacs, V. Naish, B. O'Connor, C. Blaise, F. Gagné, L. Hall, V. Trudeau, and P. Martel, "No TitlAn ecotoxicological characterization of nanocrystalline cellulose (NCC)", *Nanotoxicology*, vol. 4, no. 3, pp. 255–270, 2010.

[27] N. Drogat, R. Granet, C. Le Morvan, G. Bégaud-Grimaud, P. Krausz, and V. Sol, "Chlorin-PEI-labeled cellulose nanocrystals: Synthesis, characterization and potential application in PDT", *Bioorg. Med. Chem. Lett.*, vol. 22, no. 11, pp. 3648–3652, 2012.

[28] J. K. Jackson, K. Letchford, B. Z. Wasserman, L. Ye, W. Y. Hamad, and H. M. Burt, "The use of nanocrystalline cellulose for the binding and controlled release of drugs", *Int. J. Nanomedicine*, vol. 6, pp. 321–30, 2011.

[29] B. O′Connor, "NCC: Environmental Health and Safety Update. 2012 TAPPI Nanotechnology Conference for Renewable Materials, Montréal, QC, June 4–7, Abstract 1837", 2012.

[30] Government of Canada and Minister of the Environment. [Online]. Available: http://gazette.gc.ca/rp-pr/p2/2012/2012-11-21/html/sor-dors229-eng.html#archived. [Accessed: 05-June-2014].

[31] M. N. Anglès and A. Dufresne, "Plasticized Starch/Tunicin Whiskers Nanocomposite Materials. 2. Mechanical Behavior", *Macromolecules*, vol. 34, no. 9, pp. 2921–2931, 2001.

[32] M. Matos Ruiz, J. Y. Cavaillé, A. Dufresne, J. F. Gérard, and C. Graillat, "Processing and characterization of new thermoset nanocomposites based on cellulose whiskers", *Compos. Interfaces*, vol. 7, no. 2, pp. 117–131, 2000.

[33] B. G. Rånby, "Aqueous colloidal solutions of cellulose micelles", *Acta Chem. Scand.*, vol. 3, pp. 50–649, 1949.

[34] B. G. Rånby and E. Ribi, “Über den Feinbau der Zellulose”, *Experientia*, vol. 6, no. 1, pp. 12–14, 1950.

[35] B. G. Rånby, “Fibrous macromolecular systems. Cellulose and muscle. The colloidal properties of cellulose micelles”, *Discuss. Faraday Soc.*, vol. 11, no. 0, pp. 158–164, 1951.

[36] M. M. de Souza Lima and R. Borsali, “Static and Dynamic Light Scattering from Polyelectrolyte Microcrystal Cellulose”, *Langmuir*, vol. 18, no. 4, pp. 992–996, 2002.

[37] M. Grunert and W. Winter, “Nanocomposites of Cellulose Acetate Butyrate Reinforced with Cellulose Nanocrystals”, *J. Polym. Environ.*, vol. 10, no. 1–2, pp. 27–30, 2002.

[38] J. Araki and S. Kuga, “Effect of Trace Electrolyte on Liquid Crystal Type of Cellulose Microcrystals”, *Langmuir*, vol. 17, no. 15, pp. 4493–4496, 2001.

[39] A. Hirai, O. Inui, F. Horii, and M. Tsuji, “Phase Separation Behavior in Aqueous Suspensions of Bacterial Cellulose Nanocrystals Prepared by Sulfuric Acid Treatment”, *Langmuir*, vol. 25, no. 1, pp. 497–502, 2008.

[40] Y. Habibi and A. Dufresne, “Highly Filled Bionanocomposites from Functionalized Polysaccharide Nanocrystals”, *Biomacromolecules*, vol. 9, no. 7, pp. 1974–1980, 2008.

[41] N. L. Garcia de Rodriguez, W. Thielemans, and A. Dufresne, “Sisal cellulose whiskers reinforced polyvinyl acetate nanocomposites”, *Cellulose*, vol. 13, no. 3, pp. 261–270, 2006.

[42] G. Siqueira, J. Bras, and A. Dufresne, “Cellulose Whiskers versus Microfibrils: Influence of the Nature of the Nanoparticle and its Surface Functionalization on the Thermal and Mechanical Properties of Nanocomposites”, *Biomacromolecules*, vol. 10, no. 2, pp. 425–432, 2008.

[43] J. Araki, M. Wada, and S. Kuga, “Steric Stabilization of a Cellulose Microcrystal Suspension by Poly(ethylene glycol) Grafting”, *Langmuir*, vol. 17, no. 1, pp. 21–27, 2000.

[44] X. Dong, J.-F. Revol, and D. Gray, “Effect of microcrystallite preparation conditions on the formation of colloid crystals of cellulose”, *Cellulose*, vol. 5, no. 1, pp. 19–32, 1998.

[45] B. Dodson, “Wood pulp extract stronger than carbon fiber or Kevlar ", 2012. [Online]. Available: http://www.gizmag.com/cellulose-nanocrystals-stronger-carbon-fiber-kevlar/23959/. [Accessed: 05-June-2014].

[46] S. Elazzouzi-Hafraoui, Y. Nishiyama, J.-L. Putaux, L. Heux, F. Dubreuil, and C. Rochas, “The Shape and Size Distribution of Crystalline Nanoparticles Prepared by Acid Hydrolysis of Native Cellulose”, *Biomacromolecules*, vol. 9, no. 1, pp. 57–65, 2007.

[47] M. Roman and W. T. Winter, “Effect of Sulfate Groups from Sulfuric Acid Hydrolysis on the Thermal Degradation Behavior of Bacterial Cellulose”, *Biomacromolecules*, vol. 5, no. 5, pp. 1671–1677, 2004.

[48] W. Bai, J. Holbery, and K. Li, “A technique for production of nanocrystalline cellulose with a narrow size distribution”, *Cellulose*, vol. 16, no. 3, pp. 455–465, 2009.

[49] K. Fleming, D. Gray, S. Prasannan, and S. Matthews, “Cellulose Crystallites: A New and Robust Liquid Crystalline Medium for the Measurement of Residual Dipolar Couplings”, *J. Am. Chem. Soc.*, vol. 122, no. 21, pp. 5224–5225, 2000.

[50] S. Kalia, A. Dufresne, B. M. Cherian, B. S. Kaith, L. Avérous, J. Njuguna, and E. Nassiopoulos6, “Cellulose-Based Bio- and Nanocomposites: A Review”, *Int. J. Polym. Sci.*, vol. 2011, pp. 1–35, 2011.

[51] J. Araki, M. Wada, S. Kuga, and T. Okano, “Flow properties of microcrystalline cellulose suspension prepared by acid treatment of native cellulose”, *Colloids Surfaces A Physicochem. Eng. Asp.*, vol. 142, no. 1, pp. 75–82, 1998.

[52] T. Koshizawa, “Degradation of Wood Cellulose and Cotton Linters in Phosphoric Acid”, *JAPAN TAPPI J.*, vol. 14, no. 7, p. 455, 1960.

[53] S. Camarero Espinosa, T. Kuhnt, E. J. Foster, and C. Weder, “Isolation of Thermally Stable Cellulose Nanocrystals by Phosphoric Acid Hydrolysis”, *Biomacromolecules*, vol. 14, no. 4, pp. 1223–1230, 2013.

[54] H. Sadeghifar, I. Filpponen, S. Clarke, D. Brougham, and D. Argyropoulos, “Production of cellulose nanocrystals using hydrobromic acid and click reactions on their surface”, *J. Mater. Sci.*, vol. 46, no. 22, pp. 7344–7355, 2011.

[55] A. C. W. Leung, S. Hrapovic, E. Lam, Y. Liu, K. B. Male, K. A. Mahmoud, and J. H. T. Luong, “Characteristics and Properties of Carboxylated Cellulose Nanocrystals Prepared from a Novel One-Step Procedure”, *Small*, vol. 7, no. 3, pp. 302–305, 2011.

[56] A. E. J. de Nooy, A. C. Besemer, and H. van Bekkum, “Highly selective tempo mediated oxidation of primary alcohol groups in polysaccharides”, *Recl. des Trav. Chim. des Pays-Bas*, vol. 113, no. 3, pp. 165–166, 1994.

[57] Y. Habibi, H. Chanzy, and M. Vignon, “TEMPO-mediated surface oxidation of cellulose whiskers”, *Cellulose*, vol. 13, no. 6, pp. 679–687, 2006.

[58] M. J. Sobkowicz, B. Braun, and J. R. Dorgan, “Decorating in green: surface esterification of carbon and cellulosic nanoparticles”, *Green Chem.*, vol. 11, no. 5, pp. 680–682, 2009.

[59] B. Braun and J. R. Dorgan, “Single-Step Method for the Isolation and Surface Functionalization of Cellulosic Nanowhiskers”, *Biomacromolecules*, vol. 10, no. 2, pp. 334–341, 2008.

[60] H. Yuan, Y. Nishiyama, M. Wada, and S. Kuga, “Surface Acylation of Cellulose Whiskers by Drying Aqueous Emulsion”, *Biomacromolecules*, vol. 7, no. 3, pp. 696–700, 2006.

[61] C. Goussé, H. Chanzy, G. Excoffier, L. Soubeyrand, and E. Fleury, “Stable suspensions of partially silylated cellulose whiskers dispersed in organic solvents”, *Polymer (Guildf).*, vol. 43, no. 9, pp. 2645–2651, 2002.

[62] N. Ljungberg, C. Bonini, F. Bortolussi, C. Boisson, L. Heux, and Cavaillé, “New Nanocomposite Materials Reinforced with Cellulose Whiskers in Atactic Polypropylene: Effect of Surface and Dispersion Characteristics”, *Biomacromolecules*, vol. 6, no. 5, pp. 2732–2739, 2005.

[63] A. P. Mangalam, J. Simonsen, and A. S. Benight, “Cellulose/DNA Hybrid Nanomaterials”, *Biomacromolecules*, vol. 10, no. 3, pp. 497–504, 2009.

[64] K. H. M. Kan, J. Li, K. Wijesekera, and E. D. Cranston, “Polymer-Grafted Cellulose Nanocrystals as pH-Responsive Reversible Flocculants”, *Biomacromolecules*, vol. 14, no. 9, pp. 3130–3139, 2013.

[65] N. Lin, J. Huang, and A. Dufresne, “Preparation, properties and applications of polysaccharide nanocrystals in advanced functional nanomaterials: a review”, *Nanoscale*, vol. 4, no. 11, pp. 3274–3294, 2012.

[66] J. D. Ferry, *Viscoelastic Properties of Polymers*, 3rd ed. John Wiley & Sons Inc, New York, 1980.

[67] J. D. Wright and N. A. J. M. Sommerdijk, *Sol-Gel Materials: Chemistry and Applications*. CRC Press, New York, 2000.

[68] S. Dumitriu, “Polysaccharides in Medicinal Applications”, CRC Press, New York 1996.

[69] A. E. Way, L. Hsu, K. Shanmuganathan, C. Weder, and S. J. Rowan, “pH-Responsive Cellulose Nanocrystal Gels and Nanocomposites”, *ACS Macro Lett.*, vol. 1, no. 8, pp. 1001–1006, 2012.

[70] K. E. Shopsowitz, J. A. Kelly, W. Y. Hamad, and M. J. MacLachlan, “Biopolymer Templated Glass with a Twist: Controlling the Chirality, Porosity, and Photonic Properties of Silica with Cellulose Nanocrystals”, *Adv. Funct. Mater.*, vol. 24, no. 3, pp. 327–338, 2014.

[71] K. E. Shopsowitz, H. Qi, W. Y. Hamad, and M. J. Maclachlan, “Free-standing mesoporous silica films with tunable chiral nematic structures”, *Nature*, vol. 468, no. 7322, pp. 422–5, 2010.

[72] K. E. Shopsowitz, W. Y. Hamad, and M. J. MacLachlan, “Flexible and Iridescent Chiral Nematic Mesoporous Organosilica Films”, *J. Am. Chem. Soc.*, vol. 134, no. 2, pp. 867–870, 2011.

[73] M. K. Khan, M. Giese, M. Yu, J. A. Kelly, W. Y. Hamad, and M. J. MacLachlan, “Flexible Mesoporous Photonic Resins with Tunable Chiral Nematic Structures”, *Angew. Chemie Int. Ed.*, vol. 52, no. 34, pp. 8921–8924, 2013.

[74] J. A. Kelly, A. M. Shukaliak, C. C. Y. Cheung, K. E. Shopsowitz, W. Y. Hamad, and M. J. MacLachlan, “Responsive Photonic Hydrogels Based on Nanocrystalline Cellulose”, *Angew. Chemie Int. Ed.*, vol. 52, no. 34, pp. 8912–8916, 2013.

[75] K. E. Shopsowitz, W. Y. Hamad, and M. J. MacLachlan, “Chiral Nematic Mesoporous Carbon Derived From Nanocrystalline Cellulose”, *Angew. Chemie Int. Ed.*, vol. 50, no. 46, pp. 10991–10995, 2011.

[76] M. K. Nguyen and D. S. Lee, “Injectable Biodegradable Hydrogels”, *Macromol. Biosci.*, vol. 10, no. 6, pp. 563–579, 2010.

[77] L. Yu and J. Ding, “Injectable hydrogels as unique biomedical materials”, *Chem. Soc. Rev.*, vol. 37, no. 8, pp. 1473–1481, 2008.

[78] E. Ruel-Gariépy and J.-C. Leroux, “In situ-forming hydrogels--review of temperature-sensitive systems”, *Eur. J. Pharm. Biopharm.*, vol. 58, no. 2, pp. 409–26, 2004.

[79] D. Sivakumaran, D. Maitland, and T. Hoare, “Injectable Microgel-Hydrogel Composites for Prolonged Small-Molecule Drug Delivery”, *Biomacromolecules*, vol. 12, no. 11, pp. 4112–4120, 2011.

[80] S. B. Campbell, M. Patenaude, and T. Hoare, “Injectable Superparamagnets: Highly Elastic and Degradable Poly(N-isopropylacrylamide)–Superparamagnetic Iron Oxide Nanoparticle (SPION) Composite Hydrogels”, *Biomacromolecules*, vol. 14, no. 3, pp. 644–653, 2013.

[81] M. Patenaude and T. Hoare, “Injectable, Degradable Thermoresponsive Poly(N-isopropylacrylamide) Hydrogels”, *ACS Macro Lett.*, vol. 1, no. 3, pp. 409–413, 2012.

[82] C.-H. Ahn, S. Y. Chae, Y. H. Bae, and S. W. Kim, “Biodegradable poly(ethylenimine) for plasmid DNA delivery”, *J. Control. Release*, vol. 80, no. 1–3, pp. 273–282, 2002.

[83] N. Bhattarai, H. R. Ramay, J. Gunn, F. A. Matsen, and M. Zhang, “PEG-grafted chitosan as an injectable thermosensitive hydrogel for sustained protein release”, *J. Control. Release*, vol. 103, no. 3, pp. 609–624, 2005.

[84] J. H. Cho, S.-H. Kim, K. D. Park, M. C. Jung, W. I. Yang, S. W. Han, J. Y. Noh, and J. W. Lee, “Chondrogenic differentiation of human mesenchymal stem cells using a thermosensitive poly(N-isopropylacrylamide) and water-soluble chitosan copolymer”, *Biomaterials*, vol. 25, no. 26, pp. 5743–5751, 2004.

[85] J.-P. Chen and T.-H. Cheng, “Thermo-Responsive Chitosan-graft-poly(N-isopropylacrylamide) Injectable Hydrogel for Cultivation of Chondrocytes and Meniscus Cells”, *Macromol. Biosci.*, vol. 6, no. 12, pp. 1026–1039, 2006.

[86] S. K. Agrawal, N. Sanabria-DeLong, G. N. Tew, and S. R. Bhatia, “Nanoparticle-Reinforced Associative Network Hydrogels”, *Langmuir*, vol. 24, no. 22, pp. 13148–13154, 2008.

[87] Q. Wang, R. Hou, Y. Cheng, and J. Fu, “Super-tough double-network hydrogels reinforced by covalently compositing with silica-nanoparticles”, *Soft Matter*, vol. 8, no. 22, pp. 6048–6056, 2012.

[88] W.-C. Lin, W. Fan, A. Marcellan, D. Hourdet, and C. Creton, “Large Strain and Fracture Properties of Poly(dimethylacrylamide)/Silica Hybrid Hydrogels”, *Macromolecules*, vol. 43, no. 5, pp. 2554–2563, 2010.

[89] J. Yang, F.-K. Shi, C. Gong, and X.-M. Xie, “Dual cross-linked networks hydrogels with unique swelling behavior and high mechanical strength: Based on

silica nanoparticle and hydrophobic association", *J. Colloid Interface Sci.*, vol. 381, no. 1, pp. 107–115, 2012.

[90] A. K. Gaharwar, S. A. Dammu, J. M. Canter, C.-J. Wu, and G. Schmidt, "Highly Extensible, Tough, and Elastomeric Nanocomposite Hydrogels from Poly(ethylene glycol) and Hydroxyapatite Nanoparticles", *Biomacromolecules*, vol. 12, no. 5, pp. 1641–1650, 2011.

[91] C. Miao and W. Hamad, "Cellulose reinforced polymer composites and nanocomposites: a critical review", *Cellulose*, vol. 20, no. 5, pp. 2221–2262, 2013.

[92] A. Šturcová, G. R. Davies, and S. J. Eichhorn, "Elastic Modulus and Stress-Transfer Properties of Tunicate Cellulose Whiskers", *Biomacromolecules*, vol. 6, no. 2, pp. 1055–1061, 2005.

[93] J. Yang, J.-J. Zhao, F. Xu, and R.-C. Sun, "Revealing Strong Nanocomposite Hydrogels Reinforced by Cellulose Nanocrystals: Insight into Morphologies and Interactions", *ACS Appl. Mater. Interfaces*, vol. 5, no. 24, pp. 12960–12967, 2013.

[94] T. Abitbol, T. Johnstone, T. M. Quinn, and D. G. Gray, "Reinforcement with cellulose nanocrystals of poly(vinyl alcohol) hydrogels prepared by cyclic freezing and thawing", *Soft Matter*, vol. 7, no. 6, pp. 2373–2379, 2011.

[95] X. Zhang, J. Huang, P. R. Chang, J. Li, Y. Chen, D. Wang, J. Yu, and J. Chen, "Structure and properties of polysaccharide nanocrystal-doped supramolecular hydrogels based on Cyclodextrin inclusion", *Polymer (Guildf).*, vol. 51, no. 19, pp. 4398–4407, 2010.

[96] J. Yang, C.-R. Han, J.-F. Duan, F. Xu, and R.-C. Sun, "Mechanical and Viscoelastic Properties of Cellulose Nanocrystals Reinforced Poly(ethylene glycol) Nanocomposite Hydrogels", *ACS Appl. Mater. Interfaces*, vol. 5, no. 8, pp. 3199–3207, 2013.

[97] R. Cha, Z. He, and Y. Ni, "Preparation and characterization of thermal/pH-sensitive hydrogel from carboxylated nanocrystalline cellulose", *Carbohydr. Polym.*, vol. 88, no. 2, pp. 713–718, 2012.

[98] Q. Dai and J. F. Kadla, "Effect of nanofillers on carboxymethyl cellulose/hydroxyethyl cellulose hydrogels", *J. Appl. Polym. Sci.*, vol. 114, no. 3, pp. 1664–1669, 2009.

[99] R. Dash, M. Foston, and A. J. Ragauskas, "Improving the mechanical and thermal properties of gelatin hydrogels cross-linked by cellulose nanowhiskers", *Carbohydr. Polym.*, vol. 91, no. 2, pp. 638–645, 2013.

[100] C. Zhou, Q. Wu, Y. Yue, and Q. Zhang, “Application of rod-shaped cellulose nanocrystals in polyacrylamide hydrogels”, *J. Colloid Interface Sci.*, vol. 353, no. 1, pp. 116–123, 2011.

[101] A. Hebeish, S. Farag, S. Sharaf, and T. I. Shaheen, “Thermal responsive hydrogels based on semi interpenetrating network of poly(NIPAm) and cellulose nanowhiskers”, *Carbohydr. Polym.*, vol. 102, no. 0, pp. 159–166, 2014.

[102] J. Yang, C.-R. Han, J.-F. Duan, M.-G. Ma, X.-M. Zhang, F. Xu, R.-C. Sun, and X.-M. Xie, “Studies on the properties and formation mechanism of flexible nanocomposite hydrogels from cellulose nanocrystals and poly(acrylic acid)”, *J. Mater. Chem.*, vol. 22, no. 42, pp. 22467–22480, 2012.

[103] J. R. McKee, E. A. Appel, J. Seitsonen, E. Kontturi, O. A. Scherman, and O. Ikkala, “Healable, Stable and Stiff Hydrogels: Combining Conflicting Properties Using Dynamic and Selective Three-Component Recognition with Reinforcing Cellulose Nanorods”, *Adv. Funct. Mater.*, vol. 24, no. 18, pp. 2706-2713, 2014.

[104] S. S. Kistler, “Coherent Expanded Aerogels and Jellies”, *Nature*, vol. 127, no. 3211, p. 741, 1931.

[105] N. Hüsing and U. Schubert, “Aerogels—Airy Materials: Chemistry, Structure, and Properties”, *Angew. Chemie Int. Ed.*, vol. 37, no. 1–2, pp. 22–45, 1998.

[106] G. M. Pajonk, “Aerogel catalysts”, *Appl. Catal.*, vol. 72, no. 2, pp. 217–266, 1991.

[107] H. Hirashima, C. Kojima, and H. Imai, “Application of alumina aerogels as catalysts”, *J. Sol-Gel Sci. Technol.*, vol. 8, no. 1–3, pp. 843–846, 1997.

[108] M. Reim, W. Körner, J. Manara, S. Korder, M. Arduini-Schuster, H.-P. Ebert, and J. Fricke, “Silica aerogel granulate material for thermal insulation and daylighting”, *Sol. Energy*, vol. 79, no. 2, pp. 131–139, 2005.

[109] K. Oh, D. Kim, and S. Kim, “Ultra-porous flexible PET/Aerogel blanket for sound absorption and thermal insulation”, *Fibers Polym.*, vol. 10, no. 5, pp. 731–737, 2009.

[110] Y. J. Lee, G.-P. Kim, Y. Bang, J. Yi, J. G. Seo, and I. K. Song, “Activated carbon aerogel containing graphene as electrode material for supercapacitor”, *Mater. Res. Bull.*, vol. 50, no. 0, pp. 240–245, 2014.

[111] M. Pääkkö, J. Vapaavuori, R. Silvennoinen, H. Kosonen, M. Ankerfors, T. Lindström, L. A. Berglund, and O. Ikkala, “Long and entangled native cellulose I

nanofibers allow flexible aerogels and hierarchically porous templates for functionalities", *Soft Matter*, vol. 4, no. 12, pp. 2492–2499, 2008.

[112] H. Jin, Y. Nishiyama, M. Wada, and S. Kuga, "Nanofibrillar cellulose aerogels", *Colloids Surfaces A Physicochem. Eng. Asp.*, vol. 240, no. 1–3, pp. 63–67, 2004.

[113] F. Jiang and Y.-L. Hsieh, "Amphiphilic superabsorbent cellulose nanofibril aerogels", *J. Mater. Chem. A*, vol. 2, no. 18, pp. 6337–6342, 2014.

[114] Z. Zhang, G. Sèbe, D. Rentsch, T. Zimmermann, and P. Tingaut, "Ultralightweight and Flexible Silylated Nanocellulose Sponges for the Selective Removal of Oil from Water", *Chem. Mater.*, vol. 26, no. 8, pp. 2659–2668, 2014.

[115] W. Chen, H. Yu, Q. Li, Y. Liu, and J. Li, "Ultralight and highly flexible aerogels with long cellulose I nanofibers", *Soft Matter*, vol. 7, no. 21, pp. 10360–10368, 2011.

[116] N. Cervin, C. Aulin, P. Larsson, and L. Wågberg, "Ultra porous nanocellulose aerogels as separation medium for mixtures of oil/water liquids", *Cellulose*, vol. 19, no. 2, pp. 401–410, 2012.

[117] C. Aulin, J. Netrval, L. Wågberg, and T. Lindström, "Aerogels from nanofibrillated cellulose with tunable oleophobicity", *Soft Matter*, vol. 6, no. 14, pp. 3298–3305, 2010.

[118] H. Jin, M. Kettunen, A. Laiho, H. Pynnönen, J. Paltakari, A. Marmur, O. Ikkala, and R. H. A. Ras, "Superhydrophobic and Superoleophobic Nanocellulose Aerogel Membranes as Bioinspired Cargo Carriers on Water and Oil", *Langmuir*, vol. 27, no. 5, pp. 1930–1934, 2011.

[119] M. Kettunen, R. J. Silvennoinen, N. Houbenov, A. Nykänen, J. Ruokolainen, J. Sainio, V. Pore, M. Kemell, M. Ankerfors, T. Lindström, M. Ritala, R. H. A. Ras, and O. Ikkala, "Photoswitchable Superabsorbency Based on Nanocellulose Aerogels", *Adv. Funct. Mater.*, vol. 21, no. 3, pp. 510–517, 2011.

[120] J. T. Korhonen, M. Kettunen, R. H. A. Ras, and O. Ikkala, "Hydrophobic Nanocellulose Aerogels as Floating, Sustainable, Reusable, and Recyclable Oil Absorbents", *ACS Appl. Mater. Interfaces*, vol. 3, no. 6, pp. 1813–1816, 2011.

[121] H. Sehaqui, Q. Zhou, and L. A. Berglund, "High-porosity aerogels of high specific surface area prepared from nanofibrillated cellulose (NFC)", *Compos. Sci. Technol.*, vol. 71, no. 13, pp. 1593–1599, 2011.

[122] I. Díez, P. Eronen, M. Österberg, M. B. Linder, O. Ikkala, and R. H. A. Ras, "Functionalization of Nanofibrillated Cellulose with Silver Nanoclusters: Fluorescence and Antibacterial Activity", *Macromol. Biosci.*, vol. 11, no. 9, pp. 1185–1191, 2011.

[123] E. Haimer, M. Wendland, K. Schlufter, K. Frankenfeld, P. Miethe, A. Potthast, T. Rosenau, and F. Liebner, "Loading of Bacterial Cellulose Aerogels with Bioactive Compounds by Antisolvent Precipitation with Supercritical Carbon Dioxide", *Macromol. Symp.*, vol. 294, no. 2, pp. 64–74, 2010.

[124] Z.-Y. Wu, C. Li, H.-W. Liang, J.-F. Chen, and S.-H. Yu, "Ultralight, Flexible, and Fire-Resistant Carbon Nanofiber Aerogels from Bacterial Cellulose", *Angew. Chemie Int. Ed.*, vol. 52, no. 10, pp. 2925–2929, 2013.

[125] M. Fumagalli, F. Sanchez, S. M. Boisseau, and L. Heux, "Gas-phase esterification of cellulose nanocrystal aerogels for colloidal dispersion in apolar solvents", *Soft Matter*, vol. 9, no. 47, pp. 11309–11317, 2013.

[126] L. Heath and W. Thielemans, "Cellulose nanowhisker aerogels", *Green Chem.*, vol. 12, no. 8, pp. 1448–1453, 2010.

[127] R. Dash, Y. Li, and A. J. Ragauskas, "Cellulose nanowhisker foams by freeze casting", *Carbohydr. Polym.*, vol. 88, no. 2, pp. 789–792, 2012.

[128] M. Patenaude, N. M. B. Smeets, and T. Hoare, "Designing Injectable, Covalently Cross-Linked Hydrogels for Biomedical Applications", *Macromol. Rapid Commun.*, vol. 35, no. 6, pp. 598–617, 2014.

[129] Y. Li, J. Rodrigues, and H. Tomas, "Injectable and biodegradable hydrogels: gelation, biodegradation and biomedical applications", *Chem. Soc. Rev.*, vol. 41, no. 6, pp. 2193–2221, 2012.

[130] D. A. Ossipov, S. Piskounova, O. P. Varghese, and J. Hilborn, "Functionalization of Hyaluronic Acid with Chemoselective Groups via a Disulfide-Based Protection Strategy for In Situ Formation of Mechanically Stable Hydrogels", *Biomacromolecules*, vol. 11, no. 9, pp. 2247–2254, 2010.

[131] N. M. B. Smeets, E. Bakaic, M. Patenaude, and T. Hoare, "Injectable and tunable poly(ethylene glycol) analogue hydrogels based on poly(oligoethylene glycol methacrylate)", *Chem. Commun.*, vol. 50, no. 25, pp. 3306–3309, 2014.

[132] S. C. Thomason and D. G. Kubler, "Acids as derivatives of aldehydes prepared with silver oxides", *J. Chem. Educ.*, vol. 45, no. 8, p. 546, 1968.

[133] G. H. Motlagh, A. N. Hrymak, and M. R. Thompson, “Properties of a carbon filled cyclic olefin copolymer”, *J. Polym. Sci. Part B Polym. Phys.*, vol. 45, no. 14, pp. 1808–1820, 2007.

[134] P. Pawlikowska, B. Gajkowska, and A. Orzechowski, “Mitofusin 2 (Mfn2): a key player in insulin-dependent myogenesis in vitro”, *Cell Tissue Res.*, vol. 327, no. 3, pp. 571–581, 2007.

[135] Y. Nishiyama, P. Langan, and H. Chanzy, “Crystal Structure and Hydrogen-Bonding System in Cellulose Iβ from Synchrotron X-ray and Neutron Fiber Diffraction”, *J. Am. Chem. Soc.*, vol. 124, no. 31, pp. 9074–9082, 2002.

[136] C. Aulin, S. Ahola, P. Josefsson, T. Nishino, Y. Hirose, M. Österberg, and L. Wågberg, “Nanoscale Cellulose Films with Different Crystallinities and Mesostructures—Their Surface Properties and Interaction with Water”, *Langmuir*, vol. 25, no. 13, pp. 7675–7685, 2009.

[137] D. E. Discher, D. J. Mooney, and P. W. Zandstra, “Growth Factors, Matrices, and Forces Combine and Control Stem Cells”, *Sci.* , vol. 324 , no. 5935 , pp. 1673–1677, 2009.

[138] C. M. Nimmo, S. C. Owen, and M. S. Shoichet, “Diels−Alder Click Cross-Linked Hyaluronic Acid Hydrogels for Tissue Engineering”, *Biomacromolecules*, vol. 12, no. 3, pp. 824–830, 2011.

[139] J. M. Dugan, R. F. Collins, J. E. Gough, and S. J. Eichhorn, “Oriented surfaces of adsorbed cellulose nanowhiskers promote skeletal muscle myogenesis”, *Acta Biomater.*, vol. 9, no. 1, pp. 4707–4715, 2013.

[140] H. R. Oxley, P. H. Corkhill, J. H. Fitton, and B. J. Tighe, “Macroporous hydrogels for biomedical applications: methodology and morphology”, *Biomaterials*, vol. 14, no. 14, pp. 1064–1072, 1993.

[141] K.-U. Lewandrowski, L. D. Wise, Y. J. Michael, D. J. Gresser, J. D. Trantolo, and E. D. Altobelli, *Tissue Engineering And Biodegradable Equivalents, Scientific And Clinical Applications*. CRC Press, New York, p. 832, 2002.

[142] G. Paradossi, F. Cavalieri, and E. Chiessi, “Proton fluctuations and water diffusion in dextran chemical hydrogels studied by incoherent elastic and quasielastic neutron scattering”, *Carbohydr. Res.*, vol. 340, no. 5, pp. 921–927, 2005.

[143] M. Patenaude and T. Hoare, “Injectable, Mixed Natural-Synthetic Polymer Hydrogels with Modular Properties”, *Biomacromolecules*, vol. 13, no. 2, pp. 369–378, 2012.

[144] J. Lee and Y. Deng, “The morphology and mechanical properties of layer structured cellulose microfibril foams from ice-templating methods”, *Soft Matter*, vol. 7, no. 13, pp. 6034–6040, 2011.

[145] W. J. Lyons, “Crystal Density of Native Cellulose”, *J. Chem. Phys.*, vol. 9, p. 377, 1941.

[146] F. Liebner, E. Haimer, M. Wendland, M.-A. Neouze, K. Schlufter, P. Miethe, T. Heinze, A. Potthast, and T. Rosenau, “Aerogels from Unaltered Bacterial Cellulose: Application of scCO2 Drying for the Preparation of Shaped, Ultra-Lightweight Cellulosic Aerogels”, *Macromol. Biosci.*, vol. 10, no. 4, pp. 349–352, 2010.

[147] H.-W. Liang, Q.-F. Guan, L.-F. Chen, Z. Zhu, W.-J. Zhang, and S.-H. Yu, “Macroscopic-Scale Template Synthesis of Robust Carbonaceous Nanofiber Hydrogels and Aerogels and Their Applications”, *Angew. Chemie Int. Ed.*, vol. 51, no. 21, pp. 5101–5105, 2012.

[148] E. D. Cranston, M. Eita, E. Johansson, J. Netrval, M. Salajková, H. Arwin, and L. Wågberg, “Determination of Young’s Modulus for Nanofibrillated Cellulose Multilayer Thin Films Using Buckling Mechanics”, *Biomacromolecules*, vol. 12, no. 4, pp. 961–969, 2011.

[149] W. Zhang, Y. Zhang, C. Lu, and Y. Deng, “Aerogels from crosslinked cellulose nano/micro-fibrils and their fast shape recovery property in water”, *J. Mater. Chem.*, vol. 22, no. 23, pp. 11642–11650, 2012.

Appendices

Appendix A: Additional Data for Hydrogels

Figures A.1, A.2 and A.3 show the Fourier transform infrared (FTIR) spectroscopy results, qualitatively supporting the functionalization of the hydrogel polysaccharides. CMC-$NHNH_2$ (Figure A.1) showed unique peaks at 1620 cm^{-1} for the carbonyl group for the amide linkage between ADH and CMC and 1242 cm^{-1} for the acetate group. Dextran-CHO (Figure A.2) showed a unique peak at 1700 cm^{-1} for the carbonyl group in the aldehyde. CHO-CNCs (Figure A.3) showed unique peaks at 1640 cm^{-1} for the carbonyl group in the aldehyde and 2850 cm^{-1} for the aldehyde proton.

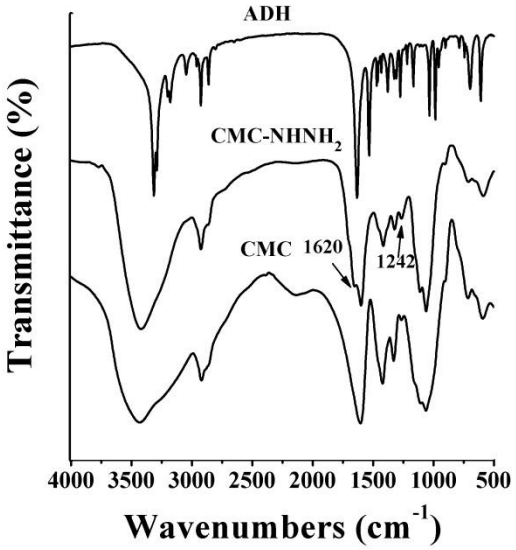

Figure A.1. FTIR spectra of adipic acid dihydrazide (ADH), CMC and CMC-$NHNH_2$.

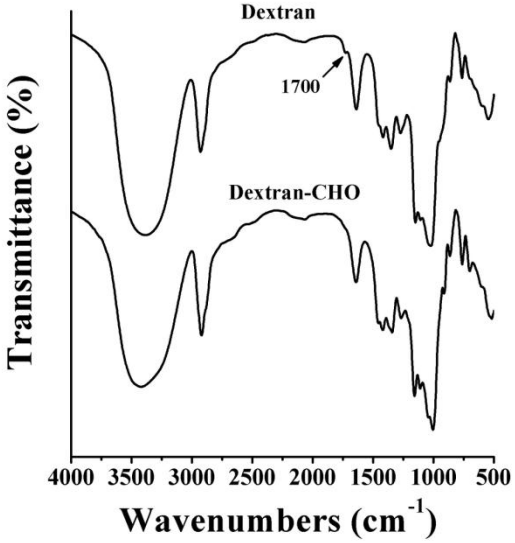

Figure A.2. FTIR spectra of dextran and dextran-CHO.

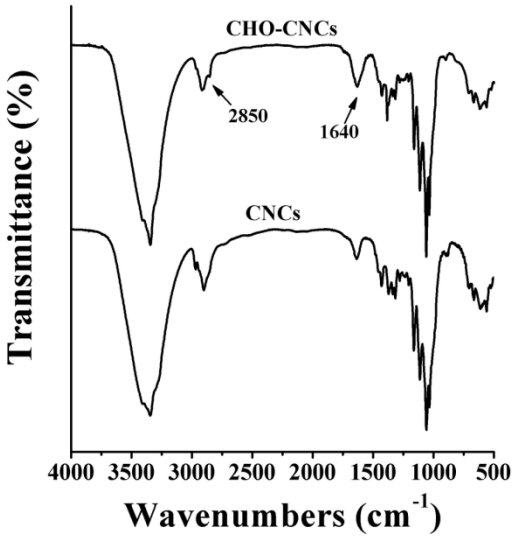

Figure A.3. FTIR spectra of CNCs and CHO-CNCs.

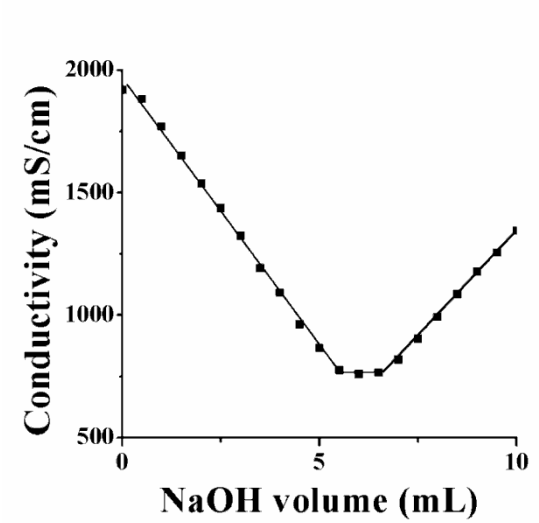

Figure A.4. Example of a titration curve used to determine aldehyde content in CHO-CNCs.

Thermogravimetric analysis (TGA) measurements were performed using a thermoanalyzer (Netzsch STA-409, Burlington, MA). 20-25 mg of lyophilized CNCs and CHO-CNCs were heated to 800 °C under air, with a 10 °C/min heating rate. CHO-CNCs were more thermally stable than "bare" acid-form CNCs, which are known to degrade at lower temperatures than sodium-form CNCs because the protonated surface sulfate ester groups can catalyze acid hydrolysis and degradation of CNCs at elevated temperatures [47]. The addition of heat stable aldehyde groups on CNCs and the slight observed reduction in the surface sulfate ester content (zeta potential increased from -37 ± 2 mV to -31 ± 2 mV after functionalization) results in the onset of thermal degradation being increased by ~14 ^{o}C.

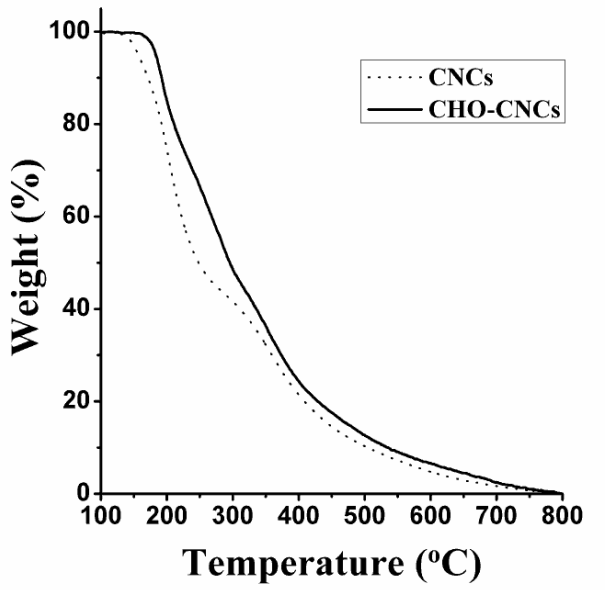

Figure A.5. TGA curves for "bare" acid-form CNCs (dotted line) and CHO-CNCs (solid line).

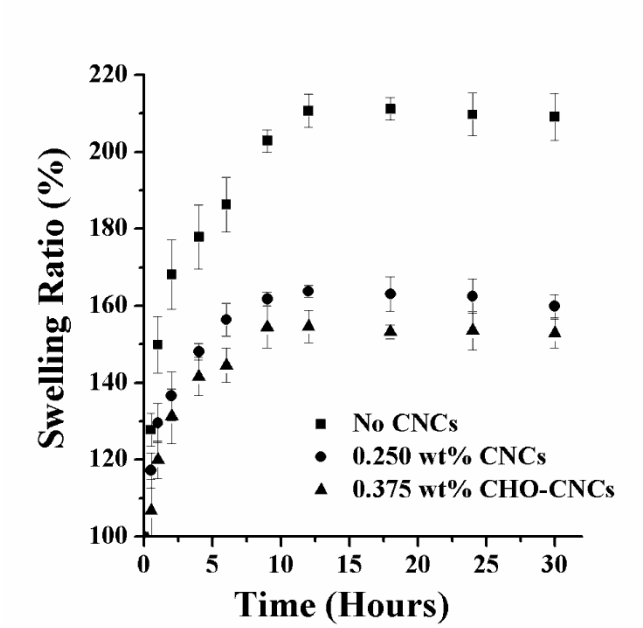

Figure A.6. Swelling of hydrogels in 10 mM PBS at 37 °C, confidence intervals are reported for $N = 4$ repeats with 95% confidence.

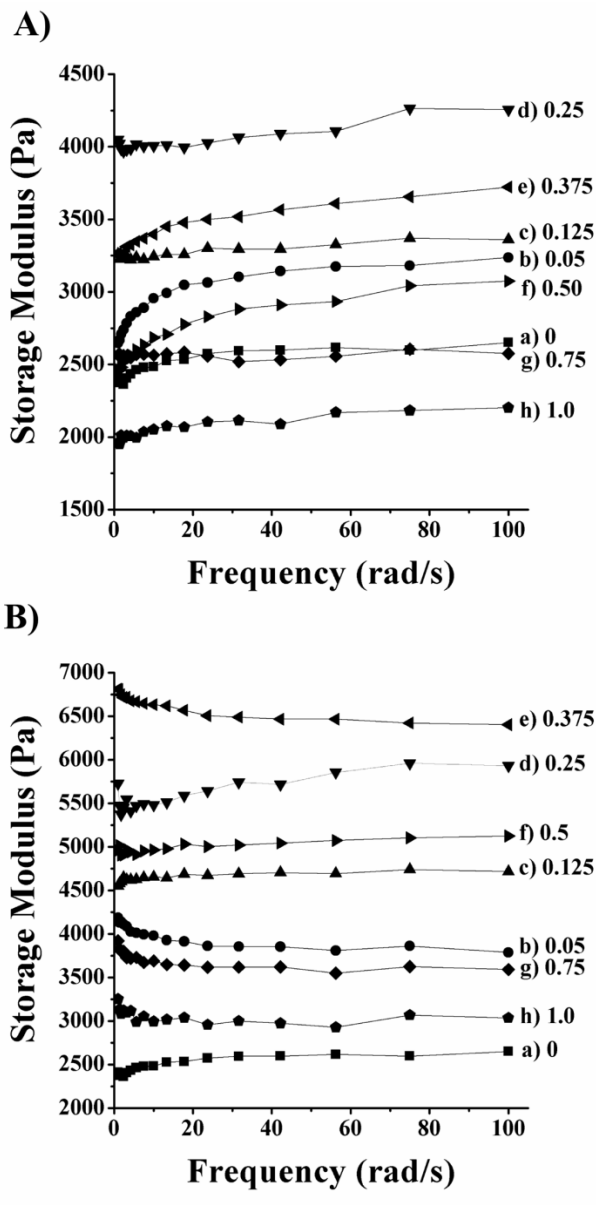

Figure A.7. Storage modulus (*G'*) as a function of frequency for (A) hydrogels with different CNC loadings; (B) hydrogels with different CHO-CNC loadings; loading concentrations in units of wt. % are listed next to their respective curve.

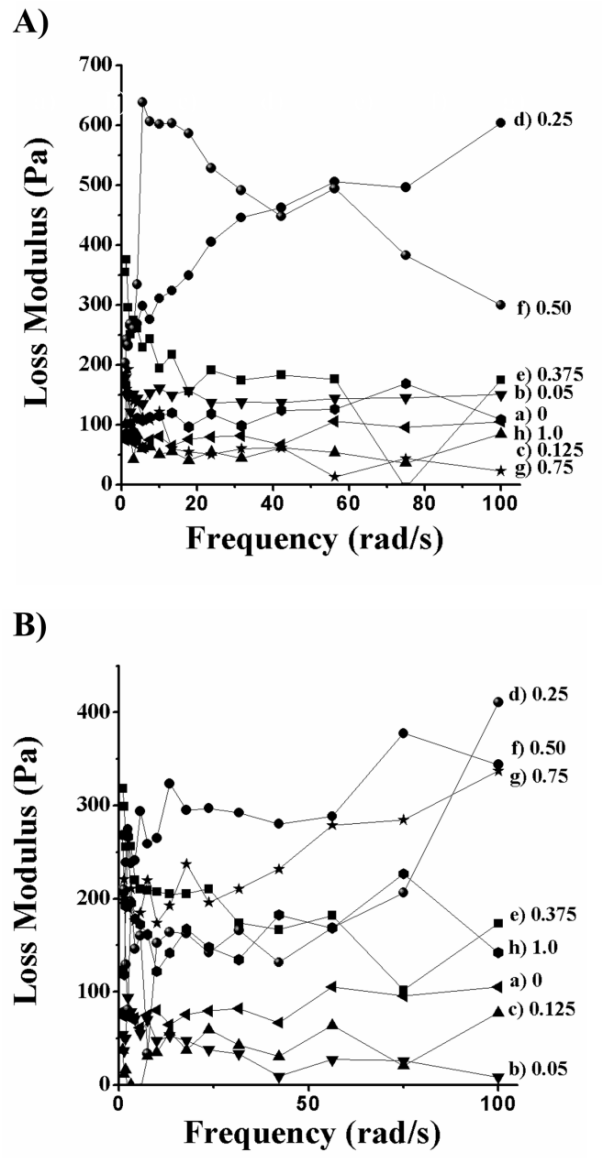

Figure A.8. Dynamic loss modulus (*G''*) as a function of frequency for (A) hydrogels with different CNC loadings; (B) hydrogels with different CHO-CNC loadings; loading concentrations in units of wt. % are listed next to their respective curve.

Appendix B: Additional Data for Aerogels

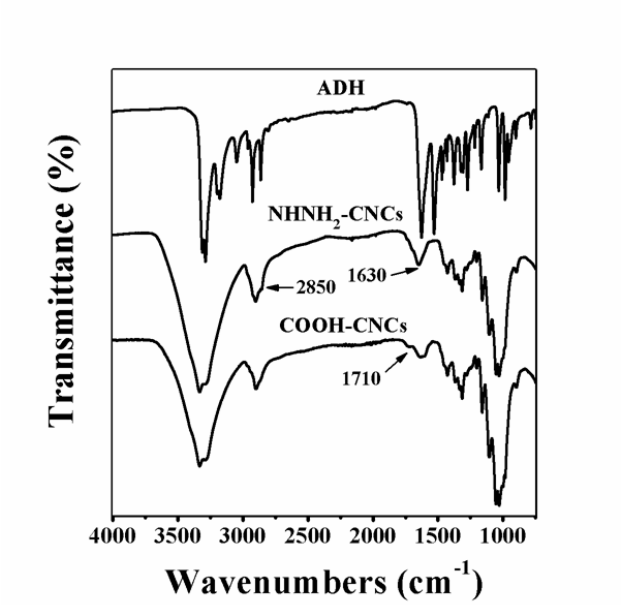

Figure B.1. FTIR spectra of adipic acid dihydrazide (ADH), $NHNH_2$-CNCs and COOH-CNCs.

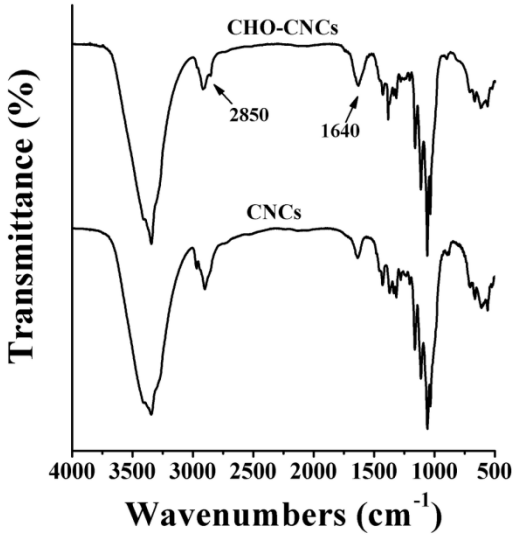

Figure B.2. FTIR spectra of CNCs and CHO-CNCs.

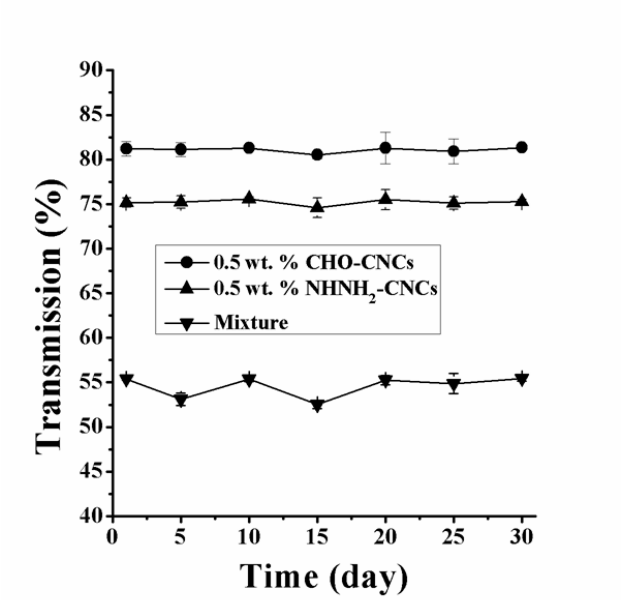

Figure B.3. UV/Visible spectroscopy transmission (turbidity) of different CNC suspensions monitored over 30 days. Confidence intervals are reported for $N = 5$ repeats with 95% confidence.